

Manuscript Number: LITHOS6733R2

Title: The Mesozoic and Palaeozoic granitoids of north-western New Guinea

Article Type: Regular Article

Keywords: Granite; Bird's Head; Gondwana; Geochronology; Zircon;  
Geochemistry

Corresponding Author: Mr. Benjamin Michael Jost, MSc.

Corresponding Author's Institution: Southeast Asia Research Group, Royal  
Holloway University of London, Egham, Surrey, UK, TW20 0EX

First Author: Benjamin Michael Jost, MSc.

Order of Authors: Benjamin Michael Jost, MSc.; Max Webb; Lloyd T White

**Abstract:** A large portion of the Bird's Head Peninsula of NW New Guinea is an inlier that reveals the pre-Cenozoic geological history of the northern margin of eastern Gondwana. The peninsula is dominated by a regional basement high exposing Gondwanan ('Australian') Palaeozoic metasediments intruded by Palaeozoic and Mesozoic granitoids. Here, we present the first comprehensive study of these granitoids, including field and petrographic descriptions, bulk rock geochemistry, and U-Pb zircon age data. We further revise and update previous subdivisions of granitoids in the area. Most granitoids were emplaced as small to medium-scale intrusions during two episodes in the Devonian-Carboniferous and the Late Permian-Triassic, separated by a period of apparent magmatic quiescence. The oldest rocks went unrecognised until this study, likely due to the younger intrusive events resetting the K-Ar isotopic system used in previous studies. Most of the Palaeozoic and Mesozoic granitoids are peraluminous and in large parts derived from partial melts of the country rock. This is corroborated by local migmatites and country rock xenoliths. Although rare, the metaluminous and mafic rocks show that partial melts of mantle-derived material played a minor role in granitoid petrogenesis, especially during the Permian-Triassic. The Devonian-Carboniferous granitoids and associated volcanics are locally restricted, whereas the Permian-Triassic intrusions are found across NW New Guinea and further afield. The latter were likely part of an extensive active continental margin above a subduction system spanning the length of what is now New Guinea and likely extending southward through eastern Australia and Antarctica.

**1 ABSTRACT**

2 A large portion of the Bird's Head Peninsula of NW New Guinea is an inlier that reveals the pre-Cenozoic  
3 geological history of the northern margin of eastern Gondwana. The peninsula is dominated by a regional  
4 basement high exposing Gondwanan ('Australian') Palaeozoic metasediments intruded by Palaeozoic and  
5 Mesozoic granitoids. Here, we present the first comprehensive study of these granitoids, including field  
6 and petrographic descriptions, bulk rock geochemistry, and U–Pb zircon age data. We further revise and  
7 update previous subdivisions of granitoids in the area. Most granitoids were emplaced as small to  
8 medium-scale intrusions during two episodes in the Devonian–Carboniferous and the Late Permian–  
9 Triassic, separated by a period of apparent magmatic quiescence. The oldest rocks went unrecognised  
10 until this study, likely due to the younger intrusive events resetting the K–Ar isotopic system used in  
11 previous studies. Most of the Palaeozoic and Mesozoic granitoids are peraluminous and in large parts  
12 derived from partial melts of the country rock. This is corroborated by local migmatites and country rock  
13 xenoliths. Although rare, the metaluminous and mafic rocks show that partial melts of mantle-derived  
14 material played a minor role in granitoid petrogenesis, especially during the Permian–Triassic. The  
15 Devonian–Carboniferous granitoids and associated volcanics are locally restricted, whereas the Permian–  
16 Triassic intrusions are found across NW New Guinea and further afield. The latter were likely part of an  
17 extensive active continental margin above a subduction system spanning the length of what is now New  
18 Guinea and likely extending southward through eastern Australia and Antarctica.

Research highlights:

- We present the first comprehensive study of granitoids from NW New Guinea.
- Magmatism occurred in the Devonian–Carboniferous and the Permian–Triassic.
- Partial melting of the continental crust produced mainly peraluminous granitoids.
- The granitoids formed in an active continental margin setting.
- The Triassic rocks are part of an extensive igneous belt along eastern Gondwana.

1 **The Mesozoic and Palaeozoic granitoids of north-western New Guinea**

2

3 Benjamin M. Jost<sup>1\*</sup>, Max Webb<sup>1,2</sup>, Lloyd T. White<sup>1,2</sup>

4

5 1. Southeast Asia Research Group, Royal Holloway University of London, Egham, Surrey, UK, TW20  
6 0EX

7 2. GeoQuEST Research Centre, School of Earth and Environmental Sciences, University of  
8 Wollongong, Wollongong, NSW, Australia, 2522

9

10 \*Corresponding author: Benjamin Jost (benjamin.m.jost@gmail.com)

11

12 **ABSTRACT**

13 A large portion of the Bird's Head Peninsula of NW New Guinea is an inlier that reveals the pre-Cenozoic  
14 geological history of the northern margin of eastern Gondwana. The peninsula is dominated by a regional  
15 basement high exposing Gondwanan ('Australian') Palaeozoic metasediments intruded by Palaeozoic and  
16 Mesozoic granitoids. Here, we present the first comprehensive study of these granitoids, including field  
17 and petrographic descriptions, bulk rock geochemistry, and U–Pb zircon age data. We further revise and  
18 update previous subdivisions of granitoids in the area. Most granitoids were emplaced as small to  
19 medium-scale intrusions during two episodes in the Devonian–Carboniferous and the Late Permian–  
20 Triassic, separated by a period of apparent magmatic quiescence. The oldest rocks went unrecognised  
21 until this study, likely due to the younger intrusive events resetting the K–Ar isotopic system used in  
22 previous studies. Most of the Palaeozoic and Mesozoic granitoids are peraluminous and in large parts  
23 derived from partial melts of the country rock. This is corroborated by local migmatites and country rock  
24 xenoliths. Although rare, the metaluminous and mafic rocks show that partial melts of mantle-derived  
25 material played a minor role in granitoid petrogenesis, especially during the Permian–Triassic. The  
26 Devonian–Carboniferous granitoids and associated volcanics are locally restricted, whereas the Permian–  
27 Triassic intrusions are found across NW New Guinea and further afield. The latter were likely part of an  
28 extensive active continental margin above a subduction system spanning the length of what is now New  
29 Guinea and likely extending southward through eastern Australia and Antarctica.

30

31 Keywords: Granite; Bird's Head; Gondwana; Geochronology; Zircon; Geochemistry

32

### 33 **1. INTRODUCTION**

34 North-western New Guinea represents part of the northern boundary of the Australian Plate and has  
35 experienced much Eocene to Recent tectonic activity (Fig. 1A; e.g., Baldwin et al., 2012; Davies, 2012; Hall,  
36 2012; Pigram and Davies, 1987). While many young tectonic features are reported from the region, such  
37 as Miocene–Pliocene high-pressure metamorphic rocks (Bailly et al., 2009; François et al., 2016) and the  
38 world's youngest ultrahigh-temperature granulites (16 Ma, Pownall et al., 2014), not much is known about  
39 the earlier, pre-Cenozoic history of the area.

40

41 Some of the oldest rocks in eastern Indonesia are exposed in NW New Guinea (commonly referred to as  
42 the Bird's Head Peninsula). These Palaeozoic and Mesozoic rocks are exposed in an extensive basement  
43 high and consist of a succession of metasedimentary basement rocks punctured by granitoid intrusions  
44 (Fig. 1B; e.g., Dow et al., 1988; Pieters et al., 1983; Visser and Hermes, 1962). These rocks are considered  
45 to represent the continuation of rocks found further south in Australia along what was then part of the  
46 northern margin of eastern Gondwana (e.g., Australasian Petroleum Company, 1961; Bladon, 1988;  
47 Charlton, 2001; Crowhurst et al., 2004; Hill and Hall, 2003; Pieters et al., 1983). Yet, we still know  
48 relatively little about the Palaeozoic–Mesozoic rocks in NW New Guinea, as geological fieldwork is  
49 complicated by remoteness, difficult access, and poor exposure. Most of what is known about the area  
50 stems from field campaigns led by the Dutch Petroleum Association summarised by Visser and Hermes  
51 (1962) and a joint Indonesian–Australian mapping project in the 1970s and 1980s (cf. compilations of  
52 Dow et al., 1988; Pieters et al., 1983).

53

54 To address this relative lack of information, we present the first comprehensive field and petrographic  
55 descriptions, bulk-rock geochemistry, and U–Pb zircon geochronology of the Palaeozoic–Mesozoic  
56 granitoids of NW New Guinea. Recent road construction and development have increased accessibility and  
57 exposure, allowing more detailed and coherent fieldwork in parts of the region. Apart from the results of a  
58 recent study of the Netoni Intrusive Complex (Fig. 1, Webb and White, 2016), the only other isotopic age  
59 control on the timing of magmatism in this region are K–Ar ages from 19 samples (Bladon, 1988; Dow et  
60 al., 1988). None of these K–Ar ages have been formally published, some lack associated uncertainties or

61 sampling locations, and 14 were determined on alluvial boulders collected from river detritus (a common  
62 last resort in remote rainforest locations where few exposures exist). Today, a broader range of more  
63 suitable geochronological techniques are available to measure the crystallisation age of igneous rocks. In  
64 summary, the aims of this study were to: (1) present the first encompassing petrographic and bulk-rock  
65 geochemical data of the granitoids of NW New Guinea, (2) test and, if necessary, update previous  
66 geochronological data with another isotopic system (U–Pb within zircon), and (3) suggest a tectonic  
67 setting for the formation of the granitoids. We begin with an overview of the stratigraphic framework of  
68 the Bird’s Head Peninsula to provide context to interpretations of tectonic models proposed for granitoid  
69 petrogenesis.

70

## 71 **2. GEOLOGICAL BACKGROUND AND PREVIOUS WORK**

72 The two most noticeable geomorphological features of the Bird’s Head are two left-lateral strike-slip fault  
73 zones, the Sorong and the Ransiki fault systems, which cross-cut the northern and north-eastern parts of  
74 the peninsula, respectively (Fig. 1). These fault zones were likely active during the past ~25 Ma (Ali and  
75 Hall, 1995; Hall, 2012) and juxtapose Eocene–Miocene volcanic arc fragments to the north and north-west  
76 with older sections of Gondwanan (‘Australian’) material to the south and south-west (e.g., Pieters et al.,  
77 1983). This Gondwanan continental crust is exposed in a large basement high, the Kemum Basement High  
78 (Fig. 1), which today forms part of the prominent mountain range of the peninsula. To the south and  
79 south-west, the basement is unconformably overlain by Palaeozoic and Mesozoic siliciclastic, Mesozoic–  
80 Miocene calcareous, and Miocene–Recent siliciclastic sediments.

81

82 Most of the granitoids that form the focus of this paper intruded country rocks exposed in the Kemum  
83 Basement High (Fig. 1B). These country rocks dominantly consist of a succession of Silurian–Devonian  
84 metaturbidites named the Kemum Formation and represent the oldest rocks in the Bird’s Head Peninsula  
85 (Visser and Hermes, 1962). Field relations indicate that the Kemum Formation was regionally  
86 metamorphosed to the lower greenschist facies before the Carboniferous (Pieters et al., 1983; Visser and  
87 Hermes, 1962). Along the eastern margin of this uplifted basement block, the rocks were later overprinted  
88 by a high-temperature/low-pressure (HT/LP) phase of metamorphism, which is speculated to be  
89 associated with the intrusion of various Permian–Triassic granitoid bodies into the eastern Kemum  
90 Basement High (Figs. 1B, 2; Dow et al., 1988; Pieters et al., 1983; 1990; Robinson et al., 1990c). The

91 intrusive bodies along this eastern margin have previously been grouped into three granitoid units: the  
92 Permian Warjori Granite, the Triassic Wariki Granodiorite, and the Triassic Anggi Granite. Table 1  
93 summarises previous knowledge of all granitoid units relevant to this study; a concise and comprehensive  
94 description of all the units based on previous work is provided in Supplementary Data File 1. At its  
95 western termination, the Kemum Formation is cross-cut by the Melaiurna Rhyolite (new name; originally  
96 termed the Melaiurna Granite by Visser and Hermes (1962)). The Kemum Formation and Melaiurna  
97 Rhyolite are unconformably overlain by siliciclastic sediments of the Late Carboniferous–Permian Aifam  
98 Group, the oldest sedimentary unit from the Bird’s Head (Amri et al., 1990; Pigram and Sukanta, 1989).

99

100 During the Permian–Triassic, the Bird’s Head Peninsula was largely exposed above sea level, likely due to  
101 uplift associated with the development of a continental arc (Gold et al., 2017, Gunawan et al., 2012; 2014;  
102 Webb and White 2016). One product of this arc is the Netoni Intrusive Complex, a granitoid complex  
103 entirely fault-bounded by the Sorong Fault System to the north of the Kemum Basement High (Fig. 1). The  
104 complex was recently described by Webb and White (2016) and consists of granite, granodiorite, quartz  
105 monzonite, and quartz syenite with subordinate diorite, quartz diorite, and pegmatite dykes (Pieters et al.,  
106 1989; Webb and White, 2016). The granitoids are calc-alkaline and peraluminous in composition,  
107 containing xenoliths of gabbro, diorite, amphibolite, and hornblende schist (Pieters et al., 1989; Webb and  
108 White, 2016). We do not investigate this unit further in this paper, but simply refer to the existing data to  
109 draw comparisons with the other granitoids found across the peninsula. The Triassic Sorong Granite is  
110 found west of the Netoni Intrusive Complex and is also bounded by the Sorong Fault System (Fig. 1B, Tab.  
111 1; Amri et al., 1990). Arc magmatism seems to have terminated by the Late Triassic to Early Jurassic and  
112 terrestrial to shallow marine deposition resumed (i.e., Late Triassic–Jurassic Tipuma Formation, Fig. 2;  
113 Gold et al., 2017; Gunawan et al., 2012; 2014, Pieters et al., 1983; Visser and Hermes, 1962).

114

115 The Bird’s Head Peninsula is connected to mainland New Guinea via the arcuate ‘Bird’s Neck’ isthmus (Fig.  
116 1). The post-Mesozoic geology of the Bird’s Neck is reportedly different to that of the Bird’s Head (Fig. 1B;  
117 Pieters et al., 1983; 1990). This isthmus predominantly consists of multiply folded Mesozoic–Cenozoic  
118 calcareous and siliciclastic sediments known as the Lengguru Fold Belt (Fig. 1B; e.g., Bailly et al., 2009).  
119 The deformation associated with the formation of this belt also led to the uplift of several N–S trending  
120 ridges that expose basement material. These are found east of the Lengguru Fold Belt within Cendrawasih

121 Bay and include the Wandaman Peninsula (Miocene–Pliocene high-grade metamorphic rocks) and the  
122 Kwatisore–Maransabadi Ridge (Permian–Triassic granitoids and older metasediments) (Bailly et al.,  
123 2009; Bladon, 1988; François et al., 2016; Pieters et al., 1983) (Fig. 1B). The latter comprises two more  
124 Permian–Triassic granitoid units, the Kwatisore Granite and the Maransabadi Granite (Fig. 1B, Tab. 1;  
125 Bladon, 1988; Pieters et al., 1983; Robinson et al., 1990b).

126

### 127 **3. METHODOLOGY**

#### 128 **3.1 Field work and sample collection**

129 This study is based on field observations and samples collected across the study area during ~15 weeks of  
130 fieldwork between 2013 and 2015 as well as several samples of the Maransabadi and Kwatisore granites  
131 that were provided by John Decker from a 2012 field campaign. The locations of the sample sites and  
132 other metadata are summarised in Supplementary Data File 2. Of the 56 samples examined in this study,  
133 13 were collected from the alluvium of rivers and 5 were collected from the scree below highly weathered  
134 outcrops. The alluvium was only sampled where weathering, vegetation, or difficult access did not permit  
135 the collection of fresh in-situ material. We present petrographic descriptions from 46 thin sections (cf.  
136 Supplementary Data File 3 for qualitative modal compositions); 40 bulk-rock geochemical analyses; and  
137 LA-ICP-MS U–Pb isotopic measurements of zircon from 35 samples (9 alluvial samples and 2 scree  
138 samples), 32 of which yielded a quantitative estimate for the crystallisation age of the respective  
139 granitoid. Please note that we follow the procedure of previous authors in grouping igneous rocks of  
140 similar petrographic, geochemical, and geochronological characteristics into lithostratigraphic units, even  
141 if samples were collected from seemingly unrelated intrusions.

142

#### 143 **3.2 Geochemistry**

144 Bulk rock geochemical analyses of major and trace element compositions were acquired using a 2010  
145 PANalytical sequential X-ray fluorescence spectrometer at Royal Holloway University of London (RHUL).  
146 Measurement procedures follow Thirlwall et al. (2000). Samples were crushed into 2–5 cm<sup>3</sup> fragments,  
147 wet sieved with a coarse mesh size (3.5 mm or 5.6 mm) to avoid cross-contamination, and dried.  
148 Fragments showing minimal alteration were then ground to a fine-grained powder using a tungsten  
149 carbide rotary mill. Major element analyses were performed on fusion disks after ignition of the sample  
150 powder at 1100°C for ~2 h; LiBO<sub>3</sub> was used as flux. Trace elements were analysed on 40 mm pressed

151 pellets, using a PVP-MC (Polyvinylpyrrolidone-Methyl Cellulose) gluing agent. For this, matrix corrections  
152 were calculated from the major element compositions and calibrated against up to 40 international  
153 standards. Limits of detection for the major and trace elements were determined using long-term  
154 reproducibility data. The software GCDkit 3.00 (Janoušek, 2006) was used for various calculations and  
155 plotting. Iron was measured as total  $\text{Fe}_2\text{O}_3$ , but recalculated and plotted as total FeO ( $\text{FeO}_t$ ).

156

### 157 **3.3 U–Pb zircon dating**

158 The geochronological data presented here were determined by U–Pb dating of zircon grains using laser  
159 ablation inductively coupled plasma mass spectrometry (LA-ICP-MS) at the London Geochronology  
160 Centre, University College London (UCL). Cathodoluminescence (CL) images of polished grain mounts  
161 were recorded using a Hitachi S3000 scanning electron microscope at RHUL or a Jeol8100 electron probe  
162 micro analyser at UCL to assess zircon textures (Supplementary Data File 4). The UCL ESI NWR 193 nm  
163 laser ablation system coupled to an Agilent 7700 quadrupole ICP-MS was used to analyse 40–50 zircon  
164 grains per sample (if the sample allowed). This work used the measurement parameters of Jackson et al.  
165 (2004). See Supplementary Data File 5 for further specifications.

166

167 Plešovice zircon ( $337.13 \pm 0.37$  Ma; Sláma et al., 2008) was measured as an external age standard. The LA-  
168 ICP-MS data were reduced with Iolite 2.5 (Paton et al., 2010; 2011) supplemented by the VizualAge data  
169 reduction scheme (Petrus and Kamber, 2012). In addition, TEMORA 2 ( $416.78 \pm 0.33$  Ma; Black et al.,  
170 2004) was measured as a secondary standard and treated as an unknown during data reduction. This  
171 allowed the calculation of an excess variance for each measurement session, which was subsequently  
172 propagated onto the internal uncertainties of each individual measurement of the respective session.  
173 Measurements with discordance  $\leq 10\%$  (within 1s) were treated as concordant and only the  $^{206}\text{Pb}/^{238}\text{U}$   
174 age of concordant analyses was used for further calculations (except inherited cores with a  $^{206}\text{Pb}/^{238}\text{U}$  age  
175  $>1000$  Ma, for which the  $^{207}\text{Pb}/^{206}\text{Pb}$  age is reported instead). Age interpretation and uncertainty  
176 propagation follow the community standard outlined by Horstwood et al. (2016) and age populations are  
177 assumed to be normally distributed (MSWD  $\sim 1$ ,  $p = 0.05$ ). Supplementary Data File 6 describes  
178 measurement procedures and the data treatment in more detail.

179

## 180 **4. RESULTS**

181 Our division of the igneous rocks of NW New Guinea into different lithostratigraphic units builds on  
182 associations made in previous studies (e.g., Dow, 1988; Pieters et al., 1983; 1990, Visser and Hermes,  
183 1962) but also accommodates the necessary changes required by new petrographic, geochemical, and  
184 geochronological data. Our new subdivision therefore differs from that of previous studies in some  
185 respects (and therefore differs from that shown in Table 1). This section describes our findings according  
186 to the new subdivision, the reasoning behind which is discussed in Section 5.1. See Supplementary Data  
187 File 7 for representative images of all units.

188

## 189 **4.1 Field observations and petrography**

### 190 *4.1.1 Devonian–Carboniferous*

191 The Mariam Granodiorite (new name) was sampled from two intrusions in the NE and the SE Kemum  
192 Basement High (Fig. 2). Our observations of these intrusives are restricted to intensely weathered  
193 outcrops and undercuts along gravel roads. The unit consists of a medium- to coarse-grained granodiorite,  
194 with plagioclase predominating over abundant quartz and subordinate K-feldspar. Biotite is characteristic  
195 and the only peraluminous phase present; it is often retrogressed to chlorite (Supp. Data File 7). Opaques,  
196 apatite, zircon, and titanite are common accessory phases.

197

198 The Ngemona Granite (new name) represents stocks, dykes, and sills that intrude the higher-grade  
199 Kemum Formation (Figs. 2, 3A). The name is derived from the Ngemona River, which drains Lake Giji into  
200 the Warjori River (Fig. 2). It is a medium- to coarse-grained leucogranite, consisting of quartz, plagioclase,  
201 K-feldspar (mostly microcline), primary muscovite, and often garnet and tourmaline, but lacks biotite (Fig.  
202 4A). The rocks are highly evolved and grade into medium to coarse-grained pegmatites. The pegmatites  
203 can contain varying amounts of primary muscovite, tourmaline, and rare garnet, but are often purely  
204 quartzofeldspathic. To distinguish primary from secondary muscovite the textural conditions introduced  
205 by Miller et al. (1981) were applied: Primary muscovite must (1) have a relatively coarse grain size,  
206 comparable to other phases; (2) show clear crystal terminations; (3) not enclose or not be enclosed by a  
207 mineral from which muscovite may have formed from alteration; and (4) be a constituent of an unaltered  
208 rock with clear igneous texture. Opaques, apatite, and zircon are common accessory phases; titanite is  
209 rare. Plagioclase is preferentially sericitised compared to K-feldspar and often shows core-and-mantle  
210 structures (Fig. 5A). Myrmekites are common where plagioclase has replaced K-feldspar (Fig. 5B).

211

212 The Wasiani Granite (new name) was the only igneous unit not observed in situ and, like Pieters et al.,  
213 (1990), we were restricted to a single alluvial sample (BJ92). The unit consists of leucocratic granite  
214 containing abundant quartz, plagioclase, and K-feldspar, supplemented with characteristic biotite that is  
215 partially retrogressed to chlorite (Fig. 4B). Zircon and apatite are abundant accessory minerals. Another  
216 alluvial sample of a melanocratic monzonite was found (BJ93) at the same location. This rock contains  
217 amphibole and partially retrogressed biotite next to abundant plagioclase and K-feldspar. Accessory  
218 minerals include opaques, titanite, apatite, and zircon (Fig. 4C). Along the same river transect,  
219 downstream (ENE) of where the two float samples were collected (Fig. 2), the country rock is crosscut by  
220 leucocratic pegmatite dykes (~5–120 cm thick), which were sampled in situ (BJ98, BJ104A; Fig. 4D).  
221 These pegmatites contain abundant muscovite and rare kyanite and tourmaline. One pegmatite dyke  
222 generated a narrow zone of contact metamorphism (hornfels) in the country rock that was subsequently  
223 folded and boudinaged (Fig. 3B).

224

225 The Kwok Granite (new name) is exposed in the easternmost part of the Kemum Basement High (Fig. 2)  
226 where it intrudes the highest-grade metamorphic basement rocks as dykes or small stocks, which are  
227 metres to tens of metres thick. The leucocratic granitoid contains fractured garnet, partially resorbed but  
228 likely primary muscovite, and abundant sillimanite (fibrolite) next to partially resorbed biotite, abundant  
229 retrogressed plagioclase, orthoclase, and quartz (Fig. 4E, 5C). Opaques, apatite, and zircon are common  
230 accessory phases. Fibrolite grows on biotite sheets (Fig. 5C) and seems to replace feldspars (Fig. 4E). The  
231 rock also displays a weak gneissose texture and is locally associated with coarse-grained pegmatites. In  
232 close proximity to the Kwok Granite (locality BH15-088), metapelitic metatexites are exposed, showing  
233 pockets and layers of leucosome within volumetrically dominant cordierite-bearing melanosome (Fig. 6A–  
234 B).

235

236 The Melaiurna Rhyolite (name modified to reflect the petrography) is exposed at the very western  
237 termination of the basement outcrop (Fig. 1B). While Visser and Hermes (1962) originally described this  
238 as a granite, we classify it as a volcanic rock due to its subvolcanic, porphyritic texture: phenocrysts of  
239 rounded and embayed quartz, muscovite, plagioclase, and orthoclase up to 15 cm in length are  
240 surrounded by a red, microcrystalline groundmass composed of quartz and feldspar (Fig. 4F). The

241 feldspars are almost completely replaced by sericite or clay minerals. Muscovite is marginally resorbed. In  
242 parts, veins of translucent white calcite cut the rocks (BH15-027). We did not observe any contacts with  
243 other units but walked across the covered contact to the overlying Aifam Group. This contact is likely a  
244 nonconformity, as the Aifam Group unit starts with a coarse-grained red arkose at its base that contains  
245 material derived from the Melaiurna Rhyolite. The unit then fines upwards via fine-grained sandstones  
246 into grey siltstone and black claystone. The basal arkose largely consists of components derived from the  
247 nearby rhyolite; the age of the Melaiurna Rhyolite thus provides a maximum depositional age for the  
248 Aifam Group.

249

250 Sample BJ10, collected at locality BH14-024 from the alluvium is petrographically different from all other  
251 Devonian–Carboniferous rocks. It is a mesocratic diorite, consisting mainly of plagioclase and biotite  
252 (Supp. Data File 7). The rock contains primary muscovite, indicative of a peraluminous composition. The  
253 mineral is metastable as it is only preserved when surrounded by biotite; where in contact with  
254 plagioclase, however, it is marginally replaced by a symplectitic texture. Opaques and zircon are also  
255 present. Sample BJ80 was collected from scree next to a strongly weathered outcrop of a dyke a few  
256 metres thick; it is not apparently related to the coeval Kwok Granite, as it was sampled in a different area  
257 (locality BH15-111). The sample is fresh and reveals a medium-grained leucogranite consisting of quartz,  
258 plagioclase, and muscovite with accessory garnet and tourmaline. A few grains of biotite are present but  
259 appear to be metastable. Similar to BJ10, muscovite is a primary mineral and replaced by symplectites  
260 where in contact with plagioclase (Fig. 5D).

261

262 Most of the granitoids are massive and lack magmatic foliations except at one location, where it is also  
263 cross-cut by a later shear zone (locality BH15-047). Other evidence for post-crystallisation deformation  
264 includes folded and boudinaged granite and pegmatite dykes as well as normal-separation faults  
265 displacing dykes and country rock xenoliths (Fig. 3A–B).

266

267 The granitoids also display evidence for solid-state deformation in thin section. Quartz and some of the  
268 feldspars have been subject to dynamic recrystallization. Larger, deformed grains of quartz (sometimes  
269 with chessboard subgrains and deformation lamellae) are replaced by smaller, undeformed grains (Fig.  
270 5E). Recrystallization seems to proceed mainly by grain boundary migration (GBM) recrystallization (Fig.

271 5A–B); bulging (BLG) and subgrain rotation (SGR) recrystallization are subordinate and rare, respectively.  
272 BLG recrystallization often occurs between quartz and the feldspars (Fig. 5A). The feldspars display a  
273 range of deformation or recrystallization features: Deformation twins, myrmekites, and mantle-and-core  
274 structures are common features in plagioclase within the Ngemona Granite, the Kwok Granite, and the  
275 Mariam Granodiorite (Fig. 5A–B). In sample BJ83, a fine-grained, garnet- and biotite-bearing granite,  
276 quartz blebs exsolved from microcline with flame-perthite textures (Fig. 5F). Tourmaline is often  
277 euhedral, forming long, stretched and broken crystals; primary micas are often bent, kinked, or partially  
278 resorbed. Despite the common solid-state deformation, a clear and dominant foliation was only observed  
279 in sample BJ67 (Kwok Granite).

280

#### 281 *4.1.2 Permian–Triassic*

282 A few intensely weathered and deformed outcrops of the Wariki Granodiorite (revised unit) were  
283 observed during a river transect into the NE Kemum Basement High (locality BH14-17). Sample BJ02  
284 likely represents a weathered granodiorite characterised by chlorite after biotite and secondary,  
285 interstitial muscovite. It is associated with quartzofeldspathic pegmatite or leucogranite dykes (Fig. 4G)  
286 that intrude the country rocks that are different from the metapelites associated with Devonian–  
287 Carboniferous granitoids. The country rocks encompass steeply dipping, black slates and layered,  
288 amphibole-bearing, and quartz-rich rocks that we tentatively interpret as low-grade metavolcanic rocks.  
289 The granodiorites are pervasively brittlely deformed and cut by several faults of various orientations. In  
290 thin section, brittle deformation (cataclasis, fracturing, kinking) is ubiquitous and predominates over  
291 ductile deformation (BLG recrystallization in quartz, deformation twins in plagioclase) (Fig. 4G). Just a few  
292 kilometres to the SW are exposures of the Mariam Granodiorite, which lack structures indicating  
293 pervasive brittle deformation.

294

295 The Anggi Intrusive Complex (revised unit) is exposed in the SE of the Kemum Basement High (Fig. 2) and  
296 encompasses a range of lithologies. Sample BJ138 is a granite containing <1 mm garnets within sheets of  
297 biotite next to quartz, feldspar, zircon, and opaques (Fig. 4H). A diorite consisting of plagioclase and  
298 chlorite as the alteration product of biotite, titanite, and opaques is exposed at locality BH15-173 (sample  
299 BJ134; Fig. 4I). In two leucocratic diorites (BJ124, LW13-6D), hornblende reacting to chlorite, plus garnet  
300 coronae growing on biotite and quartz occur next to plagioclase, quartz, opaques, and zircon (Fig. 4J).

301 Country rock xenoliths and roof pendants are abundant (Fig. 3C–D), and garnet crystals preferentially  
302 occur in the vicinity of these. At locality BH15-174, a granite intrudes metacalcareous metasediments but  
303 contains xenoliths of a metapsammitic to metapelitic rock. Despite the apparent contrast in lithology,  
304 some of the xenoliths show bedding that dips sub-parallel to that of the country rock. Thus, it cannot be  
305 said with certainty whether the xenoliths were entrained within the magma from lower structural levels  
306 or stopped from the roof or the wall of the intrusion. The xenoliths have been stretched into pinch-and-  
307 swell structures, which were later crosscut by normal-separation faults (Fig. 3D). The unit is further  
308 associated with schlieric, metapelitic diatexites (Fig. 6C–D). Compared to the migmatites associated with  
309 the Kwok Granite, the proportion of leucosome is clearly higher and the volumetrically subordinate  
310 melanosome lacks restitic anhydrous mineral phases (such as cordierite, garnet, or orthopyroxene).

311

312 The Momi Gabbro (new name) was observed along a road section through the eastern margin of the Anggi  
313 Intrusive Complex (Fig. 2). Intrusive and structural relationships between the two units were observed at  
314 locality BH15-171, where the Momi Gabbro intermingles with and cross-cuts the Anggi Intrusive Complex  
315 (Fig. 3C). The Momi Gabbro consists of gabbro and finer-grained dolerite characterised by biotite,  
316 amphibole, and augite phenocrysts (sub-)ophitically enclosing plagioclase laths. In places, the augite  
317 crystals are overgrown by rims of amphibole (uralite) (Fig. 4K). Opaques, apatite, and zircon are common  
318 accessory phases.

319

320 Fresh exposures of the Sorong Granite were observed in quarries in hummocky terrain on the northern  
321 and eastern outskirts of Sorong City (Fig. 1B). The unit consists of a heterogeneous and porphyritic pink  
322 granite with phenocrysts of pink K-feldspar in a medium to coarse-grained groundmass containing quartz,  
323 K-feldspar, biotite, and opaques and zircon as accessory phases. Xenoliths are abundant and comprise  
324 phyllite, schist, diorite, and mafic to felsic volcanic rocks. Previously reported aplite dykes (Amri et al.,  
325 1990) were not observed, whereas medium-grained pegmatite dykes were. The pegmatite contains both  
326 deep red and white K-feldspar crystals as well as coarse quartz crystals with possible garnet inclusions  
327 (Supp. Data File 7). The dykes show a sharp contact with the lighter pink main granite body. Many  
328 outcrops display intense cataclastic deformation producing large aggregates of brecciated quartz or  
329 feldspar surrounded by fine-grained granite; this deformation is likely associated with movement along  
330 the Sorong Fault System.

331

332 The Maransabadi Granite is exposed on the eponymous small island to the east of the Bird's Head  
333 Peninsula (Fig. 1B). The unit consists of medium-grained granite and granodiorite composed of quartz,  
334 partially sericitised plagioclase and K-feldspar, chlorite as the alteration product of biotite, and opaques,  
335 apatite, zircon, and titanite as accessory phases (Supp. Data File 7).

336

337 The Kwatisore Granite is exposed over a large area in the south-eastern Bird's Neck (Fig. 1B). Our samples  
338 stem from the Kwatisore Peninsula at the margin of what might be a large pluton judging from the  
339 geological map (Robinson et al., 1990e). As only the margin of this pluton was observed, the samples are  
340 not considered representative of the whole unit. They comprise a granite and a granodiorite, both  
341 medium-grained, with biotite (retrogressed to chlorite) (Fig. 4L). The rocks contain accessory titanite,  
342 zircon, apatite, and opaque phases; the granodiorite also features amphibole and secondary calcite.

343

## 344 **4.2 Geochemistry**

### 345 *4.2.1 Devonian–Carboniferous*

346 In terms of major elements, the granites and pegmatites from the Ngemona and Wasiani granites are  
347 characterised by very high and restricted SiO<sub>2</sub> contents (74–76 wt.%), only little FeO<sub>t</sub>, MgO, CaO, and TiO<sub>2</sub>,  
348 and variable Na<sub>2</sub>O and K<sub>2</sub>O (Fig. 7, Supplementary Data File 8). The Mariam Granodiorite (65–70 wt.%  
349 SiO<sub>2</sub>) exhibits the same trends, but less pronounced. The major element composition of the Kwok Granite  
350 (BJ67) and sample BJ80 is similar to that of the Ngemona and Wasiani granites, except that they are  
351 slightly less acidic (72–73 wt.% SiO<sub>2</sub>, Fig. 7). The Melaiurna Rhyolite ranges from 73 to 77 wt.% SiO<sub>2</sub>, and  
352 is enriched in FeO<sub>t</sub>, MgO, K<sub>2</sub>O, and TiO<sub>2</sub> relative to other samples of similar silica content. All rocks of these  
353 units have a comparable and relatively high Al<sub>2</sub>O<sub>3</sub> content of 12–17 wt.%. Diorite BJ10 and monzonite  
354 BJ93 are distinctly more basic (55 and 51 wt.% SiO<sub>2</sub>, respectively), richer in FeO<sub>t</sub>, MgO, CaO, TiO<sub>2</sub>, and  
355 especially Al<sub>2</sub>O<sub>3</sub> (23 and 19 wt.%, respectively). Based on their aluminium saturation index (ASI = Al<sub>2</sub>O<sub>3</sub> /  
356 [CaO + Na<sub>2</sub>O + K<sub>2</sub>O]; Shand, 1927; Zen, 1986), all samples are peraluminous (ASI from 1.02 to 2.07) apart  
357 from monzonite BJ93, which is metaluminous (ASI = 0.87) (Fig. 8A, Supp. Data File 8). All the  
358 peraluminous samples plot in the strongly or weakly peraluminous fields of the AFM triangle by Miller  
359 (1985) (Fig. 8B).

360

361 Most of these samples show enriched trace element compositions, increasing with decreasing  
362 compatibility relative to a primitive mantle composition (Palme and O'Neill, 2014; Fig. 9). The samples of  
363 the Melaiurna Rhyolite and the Mariam Granodiorite show a relatively smooth profile with positive  
364 anomalies of Th, U, K, La, and Pb and negative anomalies of Sr, P, and Ti. Their trace element compositions  
365 are remarkably similar to that of the metamorphic country rocks. The trace element composition of the  
366 Ngemona Granite also shows similarities to the country rocks, but is depleted in Ba, La, Ce, Sr, P, Zr, and Ti,  
367 and enriched in Pb. The pegmatites associated with the Wasiani Granite (BJ98, BJ104A) differ by a  
368 negative anomaly in Nd. The trace elements of the Wasiani Granite (BJ92) are comparable to those of the  
369 Mariam Granodiorite, and monzonite BJ93 shows a relatively smooth pattern with relative depletion in K,  
370 Ta, Nb, and Ti. The Kwok Granite and pegmatite BJ80 show trace element patterns not unlike those of the  
371 Ngemona Granite, but with pronounced depletion in Ba and La, and enrichment in Rb and U. Diorite BJ10  
372 conforms nicely to the trace element composition of the Kemum Formation except for prominent  
373 enrichment in Ta and Nb. Sample BJ83 has a similar trace element composition to the Ngemona Granite.

374

#### 375 *4.2.2 Permian–Triassic*

376 The Permian–Triassic event produced different units of variable composition, ranging from the most  
377 acidic Sorong Granite (77–80 wt.% SiO<sub>2</sub>) and sample BJ138 of the Anggi Intrusive Complex (74 wt.% SiO<sub>2</sub>),  
378 to the most basic rocks of the Momi Gabbro (46–49 wt.% SiO<sub>2</sub>; Fig. 7). Regarding their major element  
379 composition, samples of the Sorong Granite are indistinguishable from the coeval granites of the Netoni  
380 Intrusive Complex (Webb and White, 2016) and the older Kwok and Ngemona granites. The Maransabadi  
381 and Kwatisore granites, the Wariki Granodiorite, as well as samples BJ134 and BJ135 of the Anggi  
382 Intrusive Complex are compositionally similar to the Mariam Granodiorite, but exhibit a larger spread in  
383 SiO<sub>2</sub> composition (60–70 wt.%). Sample BJ01 is a quartzofeldspathic pegmatite associated with the Wariki  
384 Granodiorite and contains more silica (78 wt.%). The Wariki Granodiorite (BJ02) is slightly depleted in  
385 TiO<sub>2</sub> and enriched in FeO<sub>t</sub> and P<sub>2</sub>O<sub>5</sub> relative to the other samples of similar silica content and age; sample  
386 BJ135 is richer in CaO and TiO<sub>2</sub>, but lower in Na<sub>2</sub>O and K<sub>2</sub>O. These trends are almost reversed in diorite  
387 BJ134 associated with the Anggi Intrusive Complex: relative to other samples of similar silica content (62  
388 wt.%) it contains less FeO<sub>t</sub>, K<sub>2</sub>O, and TiO<sub>2</sub>, but is strongly enriched in Na<sub>2</sub>O. The more basic, garnetiferous  
389 diorites BJ124 and LW13-6D (55–56 wt.% SiO<sub>2</sub>) are compositionally similar to sample BJ10 but are even  
390 richer in Al<sub>2</sub>O<sub>3</sub> (24–26 wt.%). The Momi Gabbro shows the highest values of FeO<sub>t</sub>, MgO, and CaO of all

391 samples presented in this study. It is the only metaluminous unit of Permian–Triassic age (ASI = 0.66–  
392 0.75); all other samples are peraluminous with ASI values from 1.01 to 1.38 (Fig. 8).

393

394 The trace element patterns of the Wariki Granodiorite (sample BJ02) and the Maransabadi and Kwatisore  
395 granites are comparable and show similarities with the Mariam Granodiorite and the metamorphic  
396 basement rocks of the Kemum Formation (Fig. 9). The granites show a slight relative depletion in Cs. The  
397 trace element patterns of the Sorong Granite are similar to those of the Ngemona Granite with relative  
398 depletion in Cs and P, and enrichment in Ba, Th, U, Nb, Zr, and Ti. Samples grouped with the Anggi  
399 Intrusive Complex show a distinct trace element pattern different from all other samples; the trends are  
400 comparable although variations are large: Th, La, Ce, Nd, Hf, Zr, and Sm are noticeably enriched, while K  
401 and Ta are slightly depleted. The Momi Gabbro shows a relatively flat trace element pattern with  
402 enrichment in Pb and Sm and depletion in Th, P, and Hf.

403

#### 404 **4.3 Geochronology**

405 Of the 35 dated samples, 32 yielded meaningful age data. These fall into two distinct episodes lasting from  
406 the Late Devonian to the Late Mississippian (363–328 Ma) and the Late Permian to the Late Triassic (257–  
407 223 Ma; Figs. 10–11). No evidence for magmatism was found for the approximately 70 Myr between these  
408 two episodes. Palaeozoic magmatism seems to have peaked in the Tournaisian (355 Ma) and the  
409 Serpukhovian (330 Ma). Samples BJ92 (Wasiani Granite), MW15-022 (Sorong Granite), and BJ58 (a  
410 weathered volcanic dyke sampled in the north-eastern Kemum Basement High; BH15-080) did not yield  
411 sufficient concordant analyses to allow the calculation of a weighted mean age. The few concordant  
412 analyses we did obtain, however, indicate that the Wasiani Granite (BJ92) is part of the Palaeozoic  
413 episode, while the other two samples (MW15-022 and BJ58) intruded in the Permian–Triassic episode  
414 (Supplementary File 9). Tera-Wasserburg diagrams for all samples are given in Supplementary Data File  
415 10 and a table summarising all weighted mean ages is given Supplementary Data File 11.

416

417 Most of the zircons analysed for this study are euhedral crystals with magmatic zonation visualised by CL  
418 imaging (Fig. 12A). A few samples, however, yielded zircons that have a different morphology and  
419 appearance in CL: for example, (1) predominantly xenomorphic grains without visible zonation (BJ93, Fig.  
420 12B), (2) broken grains that were subsequently welded together by thin metamorphic zircon (BJ02, Fig.

421 12C), and (3) eu- to anhedral grains that are noticeably CL-dark and lack apparent zonation (BJ08, Fig.  
422 12D). For the latter group, which includes samples BJ08, BJ09, and BJ80, many analyses had to be rejected  
423 during the calculation of a mean age due to a large spread in ages (Fig. 10). For these samples, still  
424 concordant younger ages become progressively more discordant: they lie on a discordia or mixing line  
425 away from the most concordant population (Supplementary Data File 12). This likely reflects partial Pb  
426 loss within several zircon grains from each of these samples. CL imagery further indicates that some of the  
427 analysed zircon grains are composed of magmatic overgrowths on rounded inherited cores, some of  
428 which yielded concordant Early Palaeozoic and Proterozoic ages (Fig. 12E–H).

429

## 430 **5. DISCUSSION**

### 431 **5.1 Subdivisions of igneous rocks**

432 Several new units have been defined and some of the previous units re-named or re-defined to  
433 accommodate the data presented here: the Mariam Granodiorite and the Ngemona, Wasiani, and Kwok  
434 granites reflect the newly recognised Palaeozoic granitoids, the Momi Gabbro refers to newly found mafic  
435 rocks associated with the Anggi Intrusive Complex, and the Melaiurna Rhyolite accounts for the  
436 hypabyssal nature of the previous ‘Melaiurna Granite’ (Amri et al., 1990; Visser and Hermes, 1962). But  
437 please note that, like previous authors (e.g., Pieters et al., 1990), we use some of these names (i.e., Anggi  
438 Intrusive Complex, Mariam Granodiorite, Ngemona Granite, Wasiani Granite) collectively for different  
439 igneous rocks found in certain areas that could not be clearly subdivided due to limited field observations.  
440 There are also several samples or localities that were not classified to a particular intrusive unit, mainly  
441 because of insufficient data (this includes samples BJ10, BJ80, and BJ83 and the tentative allocation of  
442 monzonite BJ93 to the Wasiani Granite).

443

### 444 **5.2 Episodes of magmatism**

445 Carboniferous (329–328 Ma) and Permian–Triassic (257–223 Ma) magmatism was recognised and  
446 described by previous workers (e.g., Bladon, 1988; Tab. 1), but ages corresponding to the oldest rocks  
447 reported here (~355 Ma) have not been reported previously. This might reflect a sampling bias: As  
448 previous authors collected all but one of their samples from the alluvium (Bladon, 1988), we can never be  
449 sure that we dated exactly the same granitoid units they did. The ages previously reported for the Anggi  
450 Granite (as defined by Pieters et al. (1983; 1990)) agree with the U–Pb ages of the Anggi Intrusive

451 Complex (as defined here). However, for the Wariki Granodiorite, Bladon (1988) reported five Permian–  
452 Triassic ages from an area, where we also found Devonian–Carboniferous ages of the Mariam Granodiorite  
453 next to one sample of the Late Permian Wariki Granodiorite (sample BJ02). Also, U–Pb ages of the  
454 granitoids in the higher-grade Kemum Formation north of lakes Giji and Gida (cf. Fig. 2) are exclusively  
455 Palaeozoic (with the exception of sample BJ58) and apparently contradict to the Permian–Triassic ages  
456 reported in Dow et al. (1988). Such discrepancies between the ages of previous studies and those  
457 presented here cannot be explained by a sampling bias.

458

459 The potential discrepancy between ages reported here and those of previous authors (Bladon, 1988; Dow  
460 et al., 1988) for the same granitoid unit could be due to resetting the K–Ar system by (1) intense alteration  
461 or (2) a thermal event. We assume that the K-bearing minerals previously dated from alluvial samples (as  
462 summarised in Bladon, 1988) were likely less altered and led to reliable K–Ar ages, as alluvial samples are  
463 always fresh and resistant to weathering, compared to granitoid outcrops, which are often intensely  
464 weathered. The resetting of the K–Ar system by a thermal event on the other hand is more likely due to a  
465 number of reasons: (1) the extensive Permian–Triassic magmatism (Figs. 1, 2, 11); (2) a regional HT/LP  
466 metamorphic event (Pieters et al., 1990) with mineral assemblages suggesting temperatures in excess of  
467 500°C; (3) the fact that previous K–Ar ages were predominantly obtained from biotite, muscovite, and  
468 plagioclase (n = 24), which have lower closure temperatures for Ar than hornblende (n = 6) (e.g., Reiners  
469 et al., 2005 and references therein); and (4) that previous authors themselves assumed that some of their  
470 samples had been thermally disturbed and thus likely reset (Bladon, 1988). We therefore propose that the  
471 thermal anomaly caused by the intrusion of the Permian–Triassic granitoids reset the K–Ar system of  
472 older granitoids in the eastern Kemum Basement High, without this affecting their zircon U–Pb age.

473

474 This is supported by microstructural observations, most of which stem from Devonian–Carboniferous  
475 granitoids, and all of which indicate recovery and recrystallization at high temperatures (>400 °C) and  
476 low strain rates (<10<sup>-14</sup> s<sup>-1</sup>). Low strain rates are indicated by the absence of foliations, the scarceness of  
477 elongated subgrains, as well as the predominance of grain boundary migration recrystallization over  
478 bulging and subgrain rotation recrystallization in quartz. The type of dynamic recrystallization in quartz  
479 depends on both strain rate and temperature and serves as a first-order temperature gauge (e.g.,  
480 Passchier and Trouw, 2005): GBM recrystallization in quartz occurs above 400–500°C at low strain rates

481 (Stipp et al., 2002a; 2002b). Also, chessboard subgrains in quartz only develop above ~570°C at 1 kbar,  
482 and even higher temperatures at higher pressures (Kruhl, 1996). Bulbous myrmekites (Fig. 6F) also  
483 indicate recrystallization of the granitoids at similar metamorphic conditions (e.g., Phillips, 1980).  
484 Although recrystallization can be a response to syn- or post-intrusive deformation of a cooling granitoid  
485 body (e.g., Pennacchioni and Zucchi, 2013), a thermal overprint of older intrusive rocks in the eastern  
486 Kemum Basement High is likely as is indicated by the significant Permian–Triassic magmatism and  
487 concomitant regional HT/LP metamorphism (e.g., Pieters et al., 1990).

488

489 As previous authors (e.g., Dow et al., 1988; Pieters et al., 1983; 1990) underestimated the diversity of ages  
490 of granitoids from western New Guinea, it is possible that we have unintentionally done the same. A case  
491 in point is the apparent ‘magmatic gap’ during much of the Permian implied by our analyses (Fig. 13). This  
492 potentially reflects a sampling bias, particularly since a relatively small area of the Kemum Basement High  
493 was sampled. We must also consider that there has been uplift of the region since the Miocene  
494 accompanied by high erosion rates (Pieters et al., 1990), so there may be igneous bodies that have not yet  
495 been exposed at the surface or have already mostly been eroded away. Readers should also note that  
496 Permian ages were previously reported for the Warjori Granite (Bladon, 1988; Pieters et al., 1990) and for  
497 igneous rocks in the south of mainland New Guinea (Fig. 13). Detrital zircons from sedimentary rocks  
498 across the Bird’s Head Peninsula have also yielded Permian ages (Decker et al., 2017; Gunawan, 2013).  
499 Future work may therefore reveal a local source of igneous zircons of Permian or other age.

500

### 501 **5.3 Petrogenesis**

502 The weakly to highly peraluminous mineralogy and chemistry of most granitoids of NW New Guinea  
503 indicate that they are primarily derived from partial melts of the metapsammitic to metapelitic country  
504 rock and can thus be considered S-type granitoids (Chappell and White, 1974; 1992; 2001). Partial  
505 melting of continental crustal material is supported by migmatites associated with the Kwok Granite and  
506 the Anggi Intrusive Complex, which indicate incipient and pervasive partial melting, respectively (Fig. 6).  
507 As migmatization is not confined to the contact with intrusions, they are likely the result of regional  
508 HT/LP metamorphism as opposed to contact metamorphism. Also, abundant metasedimentary xenoliths  
509 in the Anggi Intrusive Complex corroborate the assimilation of and contamination with continental crustal  
510 material (Fig. 3C–D). The xenomorphic to skeletal appearance of garnets in the Anggi Intrusive Complex,

511 their association with biotite (Fig. 4H, J), the abundance of biotite and quartz inclusions within them, and  
512 their seemingly preferred occurrence around country rock xenoliths further indicates that these are  
513 restitic xenocrysts resulting from mica dehydration reactions (i.e., peritectic phases) and originated from  
514 the country rock. It is likely that the xenoliths were incorporated and contributed to the melt at greater  
515 depths (as garnet and not cordierite formed as a peritectic phase). Lastly, the presence of rounded and  
516 concordant Precambrian zircon cores (Fig. 12E–H) provides additional evidence that the petrogenesis of  
517 many of the granitoids involved partial melting of (meta)sedimentary material.

518

519 While partial melts of the continental crust significantly contributed to the petrogenesis of both the  
520 Palaeozoic and the Mesozoic magmatic events, there are petrogenetic differences between the two groups.  
521 The Devonian–Carboniferous units (Ngemona and Kwok granites, the Melaiurna Rhyolite, and the  
522 pegmatites of the Wasiani Granite) contain abundant peraluminous minerals such as muscovite, garnet,  
523 sillimanite, tourmaline, and biotite. These represent the best examples of highly peraluminous granitoids  
524 of predominantly metasedimentary origin within NW New Guinea. The Mariam Granodiorite and the  
525 Wasiani Granite (BJ92) are also peraluminous, containing biotite but lacking metaluminous minerals such  
526 as amphibole. The trace element patterns of the Mariam Granodiorite and the Melaiurna Rhyolite are also  
527 strikingly similar to those of the country rock (Fig. 9). These units are therefore interpreted to have been  
528 derived from partial melts of the continental crust. Only a few of the Devonian–Carboniferous samples  
529 slightly deviate from this trend. For example, Monzonite BJ93 is metaluminous, slightly silica  
530 undersaturated, and relatively enriched in K, HFSE, Ba, Ta, and Nb, while Samples BJ10, BJ80, and the  
531 Kwok Granite (BJ67) are enriched in Ta and Nb; the latter two also show Ti depletion. Such features are  
532 typically associated with mantle-derived within-plate magmas (Pearce, 1983; Thorpe et al., 1984).

533

534 The Permian–Triassic magmatic episode produced rocks with a more mixed signature: Many samples  
535 cannot be clearly classified as S-type granitoids, as they lack characteristic minerals and contain only  
536 mildly peraluminous biotite (Sorong Granite, Anggi Intrusive Complex, Maransabadi Granite). Further, the  
537 garnet in granites and diorites of the Anggi Intrusive Complex is likely a peritectic phase entrained from  
538 the surrounding country rock rather than a primary magmatic mineral indicative of the composition of the  
539 magma. While some of the rocks are acidic and characterised by a peraluminous modal and chemical  
540 composition (e.g., granites of the Anggi Intrusive Complex), the Kwatisore Granite and the diorites of the

541 Anggi Intrusive Complex contain amphibole, titanite, and allanite: minerals indicative of mantle-derived  
542 igneous rocks (I-type rocks; Chappell and White, 1974; 1992; 2001). Although metaluminous I-type rocks  
543 can become peraluminous via extreme fractional crystallisation, this process is considered unlikely to  
544 apply here, as large volumes of metaluminous minerals have to fractionate from the magma and  
545 peraluminous I-type granitoids can constitute only about 0.1% of the outcrop area of a pure I-type pluton  
546 (Zen, 1986). The Momi Gabbro stands out as the only mafic unit known from the Kemum Basement High.  
547 Samples BJ137 and LW13-5B are fresh and clearly metaluminous, both in terms of petrography  
548 (containing pyroxene and hornblende) and geochemistry (high FeO<sub>t</sub>, MgO, CaO; *di* normative). Trace  
549 elements show no influence of crustal contamination and only slight enrichment in LILE common of  
550 MORB or within-plate rocks (Fig. 9; Pearce, 1983). Field relations show the unit to be coeval with the  
551 Anggi Intrusive Complex, which is supported by the ages of both units (Fig. 3C).

552

553 While fractional crystallisation alone cannot explain the predominance of peraluminous rocks, it remains  
554 an important process during their petrogenesis. Fractional crystallisation of plagioclase and K-feldspar is  
555 suggested by the depletion of Sr and to a lesser degree Ba in highly evolved rocks (e.g., Ngemona, Kwok,  
556 Sorong granites and Anggi Intrusive Complex) (Brown et al., 1984). Anomalously low abundances of Ba  
557 might also be explained by the fractionation or breakdown of biotite: experimental studies indicate that  
558 tourmaline only forms in biotite-free leucogranites (e.g., Ngemona Granite) (Scaillet et al., 1995).  
559 Fractionation of garnet likely occurred in some of the pegmatites and leucosomes displaying slightly  
560 raised Sr/Y values (>30; BJ01, BJ104A, BJ135). However, this did not significantly contribute to the  
561 remaining granitoids, which are characterised by relatively low Sr/Y values (0–20), similar to the  
562 geochemical signatures of other I- or S-type granitoids or continental crustal rocks (Moyen, 2009).  
563 Fractionation of hornblende cannot be assessed satisfactorily, as Dy was not measured.

564

565 The geochemical data of the granitoids need to be interpreted with caution as some of the analysed  
566 samples show evidence of chemical weathering or metasomatic alteration. For instance, the anomalously  
567 high Na<sub>2</sub>O coupled with very low K<sub>2</sub>O and CaO contents of sample BJ134 may be indicative of albitisation  
568 (Fig. 7). The high K<sub>2</sub>O and low Na<sub>2</sub>O contents of the Melaiurna Rhyolite may also reflect potassic alteration.  
569 Features indicative such alteration (e.g., anti-rapakivi structures) are not visible in thin section due to the  
570 breakdown of the feldspars. This breakdown may also partially explain the high ASI values of the

571 Melaiurna Rhyolite and the Wariki Granodiorite (BJ02), as the alkalis are preferentially removed with  
572 respect to  $\text{Al}_2\text{O}_3$  during alteration and weathering (de la Roche, 1979). One other consideration is that  
573 many of the Palaeozoic granitoids show evidence of post-crystallisation metamorphism, which may have  
574 led to some modification of their initial composition. However, the majority of the geochemical analyses  
575 were from pristine samples, e.g., the pegmatites of the Wasiani Granite (BJ104A, BJ98), which have  
576 elevated ASI values.

577

#### 578 **5.4 Tectonic implications**

579 The granitoids exposed in the eastern Kemum Basement High likely represent the upper structural level  
580 of a magmatic system intruding at mid-crustal levels. Limited geophysical data exist for New Guinea,  
581 however, unexposed segments of the Paleozoic–Mesozoic magmatic belt are potentially imaged in gravity  
582 data processed with an upward continuation residual filter (White et al., 2014). These data show a series  
583 of zones of low gravity along the length of New Guinea beneath regions that were mapped as igneous  
584 rocks at the surface (cf., Fig. 12 from White et al., 2014). Considering the paucity of geophysical data and  
585 that numerous deformation phases have occurred since the granitoids were emplaced, our best indication  
586 for the emplacement depth comes from mineral assemblages in the metamorphic country rocks. For  
587 example, mineral assemblages characterised by andalusite and sillimanite (Pieters et al., 1983; 1990)  
588 indicate relatively low pressures (<4 kbar), corresponding to a depth of ~15 km or less. The kyanite found  
589 in pegmatite BJ104A suggests that higher pressures may have been attained, but this does not necessarily  
590 apply, as pegmatitic kyanite can form via a variety of processes other than prograde metamorphism (e.g.,  
591 Woodland, 1963). Although the pegmatites containing large proportions of hydrous phases such as  
592 muscovite and tourmaline are often associated with mid- to upper crustal levels, muscovite is  
593 thermodynamically unstable in granitic magma at pressures below 3–4 kbar (Zen, 1988). This suggests  
594 that the original melt formed at a greater depth and subsequently intruded at a shallower level. The  
595 magma also likely shifted from the stability field of muscovite, as is indicated by its sub-solidus  
596 replacement where in contact with feldspar (Fig. 5D). The presence of narrow zones of contact  
597 metamorphism around many intrusions (Fig. 3B) provides further support that hot magma was injected  
598 into shallower and cooler rocks, rather than these being derived from in-situ partial melting of and  
599 segregation from metasedimentary country rocks.

600

601 The production of large amounts of metasedimentary partial melts and regional HT/LP (Abukuma-type)  
602 metamorphism overprinting the surrounding country rocks imply a high geothermal gradient and an  
603 anomalously hot continental crust. Such regional HT/LP conditions likely accompanied both the Permian–  
604 Triassic and Devonian–Carboniferous episodes of magmatism, although the younger metamorphic phase  
605 partially overprinted the older phase. This is supported by the metapelitic migmatites associated with the  
606 Kwok Granite and the Anggi Intrusive Complex. The heat required to produce regional metamorphism and  
607 partial melting at low pressure was likely advected from the lower crust or mantle (e.g., DeYoreo et al.,  
608 1991). This potentially occurred over a relatively short-term (million-year) timescale (e.g., Viete and  
609 Lister, 2017) rather than due to long-term steady state processes and heating driven by radioactive decay  
610 (e.g., England and Thompson, 1984). This Abukuma-type metamorphism likely occurred when the region  
611 was part of an active continental arc system and heat flux to the crust was high (Fig. 13A; e.g., Gunawan et  
612 al., 2012; 2014; Metcalfe, 2013; Webb and White, 2016). This scenario is comparable to other HT/LP  
613 metamorphic terranes of the world where similar lithologies are observed, e.g., the Abukuma Plateau in  
614 Japan (e.g., Miyashiro, 1973) or the Cooma Metamorphic Complex in the Lachlan Fold Belt in SE Australia  
615 (e.g., Williams, 2001).

616  
617 This tectonic model is further supported by the trace element compositional data. For instance, the  
618 Permian–Triassic granitoids show high LILE/HFSE ratios, enrichment in Th, Rb, La, Ce, and to a lesser  
619 degree U and Ba, as well as depletion in Ta and Nb (e.g., Anggi Intrusive Complex) (Brown et al., 1984;  
620 Pearce, 1983; Thorpe et al., 1984). These rocks are dominantly calc-alkalic and magnesian in composition,  
621 characteristic of Cordilleran-type granitoids (Frost et al., 2001). The more basic Palaeozoic samples show  
622 a mixed signal with relatively enriched HFSE, Ta, and Nb indicative of a mixture between a subduction-  
623 related and a within-plate source (Brown et al., 1984; Pearce, 1983; Thorpe et al., 1984). Their Fe-rich  
624 alkali-calcic to alkalic composition is also indicative of granitoids inboard of a Cordilleran-type arc (Frost  
625 et al., 2001). We therefore interpret that the Permian–Triassic granitoids formed in an active continental  
626 margin setting above a subduction zone (Fig. 13), while the Palaeozoic granitoids are tentatively  
627 interpreted to represent post-orogenic magmatism or magmatism further inboard of an active margin.

628  
629 The Palaeozoic granitoids described above are restricted to the Bird's Head Peninsula and represent the  
630 oldest known episode of magmatism in New Guinea and eastern Indonesia (Fig. 13). These intrusives

631 represent a collection of sparse discrete exposures within the Bird's Head. They are not coeval with the  
632 Devonian to Carboniferous granitoids found in south-western New Guinea (Fig. 13; Richards and  
633 Willmott, 1970), but may potentially be part of a broader Devonian and Carboniferous orogenic belt and  
634 associated granitoid and volcanic rocks found through parts of eastern Australia and New Zealand (e.g.,  
635 Black et al., 2010; Kositcin et al., 2015; Muir et al., 1996; Raymond and Sun, 1998, and references therein).

636

637 The younger Permian–Triassic granitoids are thought to represent part of a continental arc that can be  
638 traced from as far west as the Banggai-Sula islands, through the Bird's Head Peninsula and the Bird's Neck  
639 isthmus, and eastward into mainland New Guinea (Fig. 13B). The Permian–Triassic arc is also considered  
640 to extend through eastern Gondwana (what is now eastern Australia, Zealandia and Antarctica) (Fig. 13A;  
641 Amiruddin, 2009; Charlton, 2001; Crowhurst et al., 2004; Gunawan et al., 2012; 2014; Hill and Hall, 2003;  
642 Metcalfe, 2013; Webb and White, 2016).

643

644 The arrangement of intrusive bodies in NW New Guinea is complicated and partially obliterated by  
645 sinistral strike-slip movement along the Sorong Fault System. The Netoni Intrusive Complex is probably  
646 the best example of a largely fault-bounded granitoid body in this region, and its similarity to the Wariki  
647 Granodiorite and the Anggi Intrusive Complex suggest a displacement of at least 30 km along the Sorong  
648 Fault System (Fig. 1B; Pieters et al., 1989; Webb and White, 2016). Although only few fault-bounded  
649 contacts were observed in the field, the petrographic and geochemical data presented here suggest that  
650 there are more such examples. In contrast to the granitoids of the Ngemona Granite and the Mariam  
651 Granodiorite, the Wariki Granodiorite displays abundant brittle deformation and is associated with  
652 distinct black slates and metavolcanic country rocks. This indicates that these rocks might constitute an  
653 allochthonous block that has been transported to its current location by the Ransiki and Sorong fault  
654 systems from further east, closer to the Triassic intrusions of the Anggi Intrusive Complex and the Momi  
655 Gabbro. In addition, the Sorong Granite and the Netoni Intrusive Complex are similar in age, petrography,  
656 and geochemistry and might well represent parts of the same pluton that has been dismembered and  
657 displaced by the Sorong Fault System. Further, both units are geochemically similar to the Melaiurna  
658 Rhyolite, even though the ages are different. It is feasible that the three units have a similar origin and  
659 were displaced along the major strike-slip fault system. This idea is supported by geological maps of the  
660 region showing the units with faulted contacts (Amri et al., 1990; Pieters et al., 1989; 1990).

661

**662 6. CONCLUSIONS**

663 Newly collected geochronological data show that magmatism in NW New Guinea occurred during two  
664 episodes in the Palaeozoic (Late Devonian–Late Mississippian) and the Early Mesozoic (Late Permian–  
665 Triassic). We are the first to report evidence of Devonian–Carboniferous magmatism in the Bird’s Head  
666 Peninsula, and these constitute the oldest known igneous rocks from New Guinea and eastern Indonesia.  
667 Earlier geochronological analyses of the NW New Guinea granitoids were solely based on the K–Ar  
668 method and we demonstrate that some of these measurements were potentially reset by subsequent  
669 tectono-thermal events – most likely the widespread phase of Permian–Triassic magmatism. The  
670 granitoids of NW New Guinea are predominantly evolved and peraluminous rocks that originate from  
671 partial melting of the metasedimentary continental crust (S-type granitoids). Mafic rocks (Momi Gabbro)  
672 and minor volumes of I-type rocks accompany the Permian–Triassic granitoids. These rocks likely result  
673 from magmatic activity in the continental margin above an extensive subduction zone system. A similar  
674 tectonic setting is tentatively suggested for the Devonian–Carboniferous granitoids.

675

**676 DATA AVAILIBILITY**

677 The data generated during this study are attached in the supplementary data files and are available from  
678 the EarthChem repository at (DOI link to be included upon acceptance of the manuscript).

679

**680 ACKNOWLEDGEMENTS**

681 Our thanks go to the consortium of companies who funded this research as part of the SE Asia Research  
682 Group (ENI, Murphy Oil, Repsol, Shell, Engie, Statoil, and Inpex); to John Decker and Niko Asia for donating  
683 several samples; to Roberto Dall’Agnol, Robert B. Miller, and three anonymous reviewers for helpful and  
684 constructive comments that resulted in a much improved manuscript; Robert Hall for support and helpful  
685 comments; Herwin Tiranda, Indra Gunawan, and David Gold for their invaluable contribution to  
686 fieldwork; Kevin D’Souza for hand sample photography; and Christina Manning, Matthew Thirlwall,  
687 Martin Rittner, and Andy Carter for their help in collecting geochemical and geochronological data.

688

**689 REFERENCES**

690 Ali, J.R., Hall, R., 1995. Evolution of the boundary between the Philippine Sea Plate and Australia:  
691 Palaeomagnetic evidence from eastern Indonesia. *Tectonophysics* 251, 251-275.

692

693 Amri, C., Harahap, B.H., Pieters, P.E., Bladon, G.M., 1990. The geology of the Sorong Sheet area, Irian Jaya  
694 (parts of quadrangles 2714, 2715, 2814, 2815) Scale 1: 250, 000. Geological Survey of Indonesia,  
695 Directorate of Mineral Resources, Geological Research and Development Centre, Bandung, 70pp.

696

697 Amiruddin, 2009. A Review on Permian to Triassic Active or Convergent Margin in Southeasternmost  
698 Gondwanaland: Possibility of Exploration Target for Tin and Hydrocarbon Deposits in the Eastern  
699 Indonesia. *Jurnal Geologi Indonesia* 4, 31-41.

700

701 Australasian Petroleum Company, 1961. The geological results of petroleum exploration in Western  
702 Papua. *Journal of the Geological Society of Australia* 8, 1-133.

703

704 Bailly, V., Pubellier, M., Ringenbach, J.-C., de Sigoyer, J., Sapin, F., 2009. Deformation zone 'jumps' in a  
705 young convergent setting; the Lengguru fold-and-thrust belt, New Guinea Island. *Lithos* 113, 306-317.

706

707 Baldwin, S.L., Fitzgerald, P.G., Webb, L.E., 2012. Tectonics of the New Guinea region. *Annual Review of*  
708 *Earth and Planetary Sciences* 40, 495-520.

709

710 Black, L. P., Everard, J. L., McClenaghan, M. P., Korsch, R. J., Calver, C. R., Fioretti, A. M., Brown, A.V.,  
711 Foudoulis, C., 2010. Controls on Devonian-Carboniferous magmatism in Tasmania, based on inherited  
712 zircon age patterns, Sr, Nd and Pb isotopes, and major and trace element geochemistry. *Australian Journal*  
713 *of Earth Sciences*, 57(7), 933-968.

714

715 Black, L.P., Kamo, S.L., Allen, C.M., Davis, D.W., Aleinikoff, J.N., Valley, J.W., Mundil, R., Campbell, I.H., Korsch,  
716 R.J., Williams, I.S., 2004. Improved  $^{206}\text{Pb}/^{238}\text{U}$  microprobe geochronology by the monitoring of a trace-  
717 element-related matrix effect; SHRIMP, ID-TIMS, ELA-ICP-MS and oxygen isotope documentation for a  
718 series of zircon standards. *Chemical Geology* 205, 115-140.

719

- 720 Bladon, G.M., 1988. Preliminary geological report. Catalogue, appraisal and significance of K-Ar isotopic  
721 ages determined for igneous and metamorphic rocks in Irian Jaya. Indonesia-Australia Geological Mapping  
722 Project 79pp.  
723
- 724 Brown, G.C., Thorpe, R.S., Webb, P.C., 1984. The geochemical characteristics of granitoids in contrasting  
725 arcs and comments on magma sources. *J. Geol. Soc. London.* 141, 413–426. doi:10.1144/gsjgs.141.3.0413  
726
- 727 Chappell, B.W., White, A.J.R., 1974. Two contrasting granite types. *Pacific geology* 8, 173-174.  
728
- 729 Chappell, B.W., White, A.J.R., 1992. I-and S-type granites in the Lachlan Fold Belt. *Geological Society of*  
730 *America Special Papers* 272, 1-26.  
731
- 732 Chappell, B.W., White, A.J.R., 2001. Two contrasting granite types: 25 years later. *Australian Journal of*  
733 *Earth Sciences.* 48, 489–500. doi:10.1046/j.1440-0952.2001.00882.x  
734
- 735 Charlton, T.R., 2001. Permo-Triassic evolution of Gondwanan eastern Indonesia, and the final Mesozoic  
736 separation of SE Asia from Australia. *Journal of Asian Earth Sciences* 19, 595-617.  
737
- 738 Crowhurst, P.V., Maas, R., Hill, K.C., Foster, D.A., Fanning, C.M., 2004. Isotopic constraints on crustal  
739 architecture and Permo-Triassic tectonics in New Guinea: possible links with eastern Australia. *Australian*  
740 *Journal of Earth Sciences* 51, 109-124.  
741
- 742 Davies, H.L., 1990. Structure and Evolution of the Border Region of New Guinea. In: *Petroleum Exploration*  
743 *in Papua New Guinea* (Edited by Carman, G.J. & Carman, Z.) *Proceedings of the First PNG Petroleum*  
744 *Convention* 245-270.  
745
- 746 Davies, H.L., 2012. The geology of New Guinea-the cordilleran margin of the Australian continent.  
747 *Episodes* 35, 87-102.  
748

749 de La Roche, H., 1979. Muscovitisation deutérique, caractère alumineux des leucogranites et classification  
750 des granites subsolvus. Bulletin de la Société Géologique de France 7, 87-93.

751

752 Decker, J., Ferdian, F., Morton, A., Fanning, M., White, L.T., 2017. New geochronology data from eastern  
753 Indonesia – and aid to understanding sedimentary provenance in a frontier region. Indonesian Petroleum  
754 Association, Proceedings 41th annual convention & exhibition, Jakarta, 2017.

755

756 De Yoreo, J. J., Lux, D. R., Guidotti, C. V., 1991. Thermal modelling in low-pressure/high-temperature  
757 metamorphic belts. Tectonophysics, 188(3-4), 209-238.

758

759 Dow, D.B., Robinson, G.P., Hartono, U., Ratman, N., 1988. Geology of Irian Jaya: Preliminary Geological  
760 Report. Geological Research and Development Centre - Bureau of Mineral Resources, Canberra.

761

762 Dow, D.B., Harahap, B.H., Sufni Hakim, A., 1990. Geology of the Enarotali Sheet area, Irian Jaya, Scale 1:  
763 250, 000. Geological Survey of Indonesia, Directorate of Mineral Resources, Geological Research and  
764 Development Centre, Bandung, 57pp.

765

766 Ferdian, F., Decker, J., Morton, A., Fanning, M., 2012. Provenance of East Sulawesi and Banggai Sula  
767 Zircons–Preliminary Result. Indonesian Petroleum Association, Proceedings 36th annual convention &  
768 exhibition, Jakarta, 2012.

769

770 François, C., de Sigoyer, J., Pubellier, M., Bailly, V., Cocherie, A., Ringenbach, J.-C., 2016. Short-lived  
771 subduction and exhumation in Western Papua (Wandamen peninsula): Co-existence of HP and HT  
772 metamorphic rocks in a young geodynamic setting. Lithos 266, 44-63.

773

774 Frost, B.R., Barnes, C.G., Collins, W.J., Arculus, R.J., Ellis, D.J., Frost, C.D., 2001. A geochemical classification  
775 for granitic rocks. J. Petrol. 42, 2033–2048. doi:10.1093/petrology/42.11.2033

776

- 777 Gold, D.P., White, L.T., Gunawan, I., BouDagher-Fadel, M.K., 2017. Relative sea-level change in western New  
778 Guinea recorded by regional biostratigraphic data. *Mar. Pet. Geol.* 86, 1133–1158.  
779 doi:10.1016/j.marpetgeo.2017.07.016  
780
- 781 Gradstein, F.M., Ogg, J.G., Hilgren, F.J., 2012. On the Geologic Time Scale. *Newsletters on Stratigraphy* 45,  
782 171-188.  
783
- 784 Gunawan, I., 2013. Mesozoic and Cenozoic Siliciclastic Sedimentary Rocks of the Bird's Head of New  
785 Guinea, Indonesia. Unpublished PhD thesis, SE Asia Research Group, Department of Earth Sciences, Royal  
786 Holloway University of London, 472pp.  
787
- 788 Gunawan, I., Hall, R., Augustsson, C., Armstrong, R., 2014. Quartz from the Tipuma Formation, West Papua:  
789 New insights from geochronology and cathodoluminescence studies. Indonesian Petroleum Association,  
790 Proceedings 38th annual convention & exhibition, Jakarta, 2014.  
791
- 792 Gunawan, I., Hall, R., Sevastjanova, I., 2012. Age, character and provenance of the Tipuma Formation, West  
793 Papua: New insights from detrital zircon dating. Indonesian Petroleum Association, Proceedings 36th  
794 annual convention & exhibition, Jakarta, 2012.  
795
- 796 Hall, R., 2012. Late Jurassic-Cenozoic reconstructions of the Indonesian region and the Indian Ocean.  
797 *Tectonophysics* 570, 1-41.  
798
- 799 Harding, R.R., 1969. Catalogue of Age Determinations on Australian Rocks, 1962-1965, Bureau of Mineral  
800 Resources, Geology and Geophysics.  
801
- 802 Hijmans, R., 2014. Global Administrative Areas – Boundaries without limits [web resource].  
803 <http://gadm.org/>. October 2014.  
804

805 Hill, K.C., Hall, R., 2003. Mesozoic-Cenozoic evolution of Australia's New Guinea margin in a west Pacific  
806 context. Geological Society of Australia Special Publication 22 and Geological Society of America Special  
807 Paper 372 265-289.

808

809 Horstwood, M.S.A., Košler, J., Gehrels, G., Jackson, S.E., McLean, N.M., Paton, C., Pearson, N.J., Sircombe, K.,  
810 Sylvester, P., Vermeesch, P., 2016. Community-Derived Standards for LA-ICP-MS U-(Th-) Pb  
811 Geochronology–Uncertainty Propagation, Age Interpretation and Data Reporting. *Geostandards and*  
812 *Geoanalytical Research* 40, 311-332.

813

814 Jackson, S.E., Pearson, N.J., Griffin, W.L., Belousova, E.A., 2004. The application of laser ablation-inductively  
815 coupled plasma-mass spectrometry to in situ U–Pb zircon geochronology. *Chemical Geology* 211, 47-69.

816

817 Janoušek, V., Farrow, C.M., Erban, V., 2006. Interpretation of Whole-rock Geochemical Data in Igneous  
818 Geochemistry: Introducing Geochemical Data Toolkit (GCDkit). *Journal of Petrology* 47, 1255-1259.

819

820 Kositsin, N., Purdy, D. J., Brown, D. D., Bultitude, R. J., Carr, P. A., 2015. Summary of results – Joint GSQ–GA  
821 Geochronology Project: Thomson Orogen and Hodgkinson Province, 2012–2013. *Queensland Geological*  
822 *Record* 2015/02, 75pp.

823

824 Kruhl, J.H., 1996. Prism-and basal-plane parallel subgrain boundaries in quartz: A microstructural  
825 geothermobarometer. *Journal of Metamorphic Geology* 14, 581-589.

826

827 Metcalfe, I., 2013. Tectonic evolution of the Malay Peninsula. *Journal of Asian Earth Sciences*, 76, 195-213.

828

829 Miller, C.F., 1985. Are strongly peraluminous magmas derived from pelitic sedimentary sources? *The*  
830 *Journal of Geology* 93, 673-689.

831

832 Miller, C.F., Stoddard, E.F., Bradfish, L.J., Dollase, W.A., 1981. Composition of plutonic muscovite: genetic  
833 implications. *Can. Mineral.* 19, 25–34.

834

- 835 Moyen, J.F., 2009. High Sr/Y and La/Yb ratios: the meaning of the “adakitic signature”. *Lithos*, 112, 556–  
836 574.
- 837
- 838 Muir, R. J., Ireland, T. R., Weaver, S. D., Bradshaw, J. D., 1996. Ion microprobe dating of Paleozoic  
839 granitoids: Devonian magmatism in New Zealand and correlations with Australia and Antarctica. *Chemical*  
840 *Geology*, 127(1-3), 191-210.
- 841
- 842 Norvick, M., Hutchinson, D.S., 1980. 1: 250,000 Geological series—explanatory notes: Aitape-Vanimu,  
843 Papua New Guinea. Department of Minerals and Energy, Geological Survey of Papua New Guinea, Port  
844 Moresby.
- 845
- 846 Page, R.W., 1976. Geochronology of igneous and metamorphic rocks in the New Guinea Highlands.  
847 Australian Bureau of Mineral Resources, Geology and Geophysics Bulletin 162, 117pp.
- 848
- 849 Palme, H., O'Neill, H.S.C., 2014. Cosmochemical estimates of mantle composition. *Treatise on*  
850 *geochemistry*, second edition 3, 1-39.
- 851
- 852 Panggabean, H., 1990. Geology of the Omba sheet area, Irian Jaya. Geological Survey of Indonesia,  
853 Directorate of Mineral Resources, Geological Research and Development Centre, Bandung.
- 854
- 855 Passchier, C.W., Trouw, R.A.J., 2005. *Microtectonics*. Springer, Berlin, pp. 366.
- 856
- 857 Paton, C., Hellstrom, J., Paul, B., Woodhead, J., Hergt, J., 2011. Lolite: Freeware for the visualisation and  
858 processing of mass spectrometric data. *Journal of Analytical Atomic Spectrometry* 26, 2508-2518.
- 859
- 860 Paton, C., Woodhead, J.D., Hellstrom, J.C., Hergt, J.M., Greig, A., Maas, R., 2010. Improved laser ablation U-Pb  
861 zircon geochronology through robust downhole fractionation correction. *Geochemistry, Geophysics,*  
862 *Geosystems* 11.
- 863

864 Pearce, J.A., 1983. Role of the sub-continental lithosphere in magma genesis at active continental margins,  
865 in: Hawkesworth, C.J., Nurry, M.J. (Eds.), *Continental Basalts and Mantle Xenoliths*. Shiva Publishing,  
866 Nantwich, pp. 230–249.

867

868 Pennacchioni, G., Zucchi, E., 2013. High temperature fracturing and ductile deformation during cooling of a  
869 pluton: The Lake Edison granodiorite (Sierra Nevada batholith, California). *Journal of Structural Geology*  
870 50, 54-81.

871

872 Petrus, J.A., Kamber, B.S., 2012. VizualAge: A Novel Approach to Laser Ablation ICP-MS U-Pb  
873 Geochronology Data Reduction. *Geostandards and Geoanalytical Research* 36, 247-270.

874

875 Phillips, E.R., 1980. On polygenetic myrmekite. *Geological Magazine*, 117, 29–36.

876

877 Pieters, P.E., Hakim, A.S., Atmawinata, S., 1990. *Geologi lembar Ransiki, Irian Jaya*. Geological Survey of  
878 Indonesia, Directorate of Mineral Resources, Geological Research and Development Centre, Bandung  
879 81pp.

880

881 Pieters, P.E., Hartono, U., Amri, C., 1989. *Geologi lembar Mar, Irian Jaya*. Geological Survey of Indonesia,  
882 Directorate of Mineral Resources, Geological Research and Development Centre, Bandung 62pp.

883

884 Pieters, P.E., Pigram, C.J., Trail, D.S., Dow, D.B., Ratman, N., Sukanto, R., 1983. The stratigraphy of western  
885 Irian Jaya. *Bulletin Geological Research and Development Centre, Bandung* 8, 14-48.

886

887 Pigram, C., Arnold, G.O., Griffin, T.J., 1977. *Geology of the Minj 1:100 000 Sheet area*. Geological Survey of  
888 Papua New Guinea Archives.

889

890 Pigram, C.J., Davies, H.L., 1987. Terranes and the accretion history of the New Guinea orogen. *BMR Journal*  
891 *of Australian Geology and Geophysics* 10, 193-212.

892

- 893 Pigram, C.J., Panggabean, H., 1989. Geology of the Waghete Sheet area, Irian Jaya. Geological Survey of  
894 Indonesia, Directorate of Mineral Resources, Geological Research and Development Centre, Bandung.  
895
- 896 Pigram, C.J., Sukanta, U., 1989. Geologi lembar Taminabuan, Irian Jaya. Geological Survey of Indonesia,  
897 Directorate of Mineral Resources, Geological Research and Development Centre, Bandung 51pp.  
898
- 899 Pownall, J.M., Hall, R., Armstrong, R.A., Forster, M.A., 2014. Earth's youngest known ultrahigh-temperature  
900 granulites discovered on Seram, eastern Indonesia. *Geology* 42, 279-282.  
901
- 902 Raymond, O., Sun, S. S., 1998. A comparison of Ordovician and Devonian magmatism in the eastern  
903 Lachlan Fold Belt: re-evaluating exploration targets. *AGSO Research Newsletter*, 28, 8–10.  
904
- 905 Reiners, P.W., Ehlers, T.A., Zeitler, P.K., 2005. Past, present, and future of thermochronology. *Reviews in*  
906 *Mineralogy and Geochemistry*, 58, 1–18.  
907
- 908 Richards, J.R., Wilmott, W.F., 1970. K-Ar age of biotites from Torres Strait. *Australian Journal of Science* 32.  
909
- 910 Robinson, G.P., Harahap, B.H., Suparman, M., Bladon, G.M., 1990a. Geologi lembar Fak Fak, Irian Jaya.  
911 Geological Survey of Indonesia, Directorate of Mineral Resources, Geological Research and Development  
912 Centre, Bandung 51pp.  
913
- 914 Robinson, G.P., Harahap, B.H., Tobing, S.L., Bladon, G.M., 1990b. Geologi lembar Pulau Karas-Pulau Adi,  
915 Irian Jaya. Geological Survey of Indonesia, Directorate of Mineral Resources, Geological Research and  
916 Development Centre, Bandung 39pp.  
917
- 918 Robinson, G.P., Ratman, N., Pieters, P.E., 1990c. Geology of the Manokwari sheet area, Irian Jaya. Geological  
919 Survey of Indonesia, Directorate of Mineral Resources, Geological Research and Development Centre,  
920 Bandung.  
921

- 922 Robinson, G.P., Ryburn, R.J., Harahap, B.H., Tobing, S.L., Achdan, A., Bladon, G.M., Pieters, P.E., 1990d.  
923 Geology of the Steenkool sheet area, Irian Jaya. Geological Survey of Indonesia, Directorate of Mineral  
924 Resources, Geological Research and Development Centre, Bandung.  
925
- 926 Robinson, G.P., Ryburn, R.J., Harahap, B.H., Tobing, S.L., Bladon, G.M., Pieters, P.E., 1990e. Geology of the  
927 Kaimana Sheet area, Irian Jaya. Geological Survey of Indonesia, Directorate of Mineral Resources,  
928 Geological Research and Development Centre, Bandung.  
929
- 930 Scaillet, B., Pichavant, M., Roux, J., 1995. Experimental Crystallization of Leucogranite Magmas. *J. Petrol.*  
931 36, 663–705.  
932
- 933 Shand, S.J., 1927. On the relations between silica, alumina, and the bases in eruptive rocks, considered as a  
934 means of classification. *Geological Magazine* 64, 446-449.  
935
- 936 Sláma, J., Košler, J., Condon, D.J., Crowley, J.L., Gerdes, A., Hanchar, J.M., Horstwood, M.S.A., Morris, G.A.,  
937 Nasdala, L., Norberg, N., 2008. Plešovice zircon—a new natural reference material for U–Pb and Hf  
938 isotopic microanalysis. *Chemical Geology* 249, 1-35.  
939
- 940 Stipp, M., Stünitz, H., Heilbronner, R., Schmid, S.M., 2002a. Dynamic recrystallization of quartz: correlation  
941 between natural and experimental conditions. *Geological Society, London, Special Publications* 200, 171-  
942 190.  
943
- 944 Stipp, M., Stünitz, H., Heilbronner, R., Schmid, S.M., 2002b. The eastern Tonale fault zone: a ‘natural  
945 laboratory’ for crystal plastic deformation of quartz over a temperature range from 250 to 700 C. *Journal*  
946 *of Structural Geology* 24, 1861-1884.  
947
- 948 Thirlwall, M.F., Singer, B.S., Marriner, G.F., 2000. 39 Ar–40 Ar ages and geochemistry of the basaltic shield  
949 stage of Tenerife, Canary Islands, Spain. *Journal of Volcanology and Geothermal Research* 103, 247-297.  
950

- 951 Thorpe, R.S., Francis, P.W., O'Callaghan, L., 1984. Relative roles of source composition, fractional  
952 crystallization and crustal contamination in the petrogenesis of Andean volcanic rocks. *Philos. Trans. R.*  
953 *Soc. London A* 310, 675–692.
- 954
- 955 Van Wyck, N., Williams, I.S., 2002. Age and provenance of basement metasediments from the Kubor and  
956 Bena Bena Blocks, central Highlands, Papua New Guinea: constraints on the tectonic evolution of the  
957 northern Australian cratonic margin. *Australian Journal of Earth Sciences* 49, 565-578.
- 958
- 959 Viete, D.R., Lister, G.S., 2017. On the significance of short-duration regional metamorphism. *Journal of the*  
960 *Geological Society*, 174, 377–392.
- 961
- 962 Visser, W.A., Hermes, J.J., 1962. Geological results of the exploration for oil in Netherlands New Guinea.  
963 *Verhandelingen Koninklijk Nederlands Geologisch en Mijnbouwkundig Genootschap, Geologische Serie*  
964 20, 265pp.
- 965
- 966 Webb, M., White, L.T., 2016. Age and nature of Triassic magmatism in the Netoni Intrusive Complex, West  
967 Papua, Indonesia. *Journal of Asian Earth Sciences* 132, 58-74.
- 968
- 969 White, L.T., Morse, M.P., Lister, G.S., 2014. Lithospheric-scale structures in New Guinea and their control  
970 on the location of gold and copper deposits. *Solid Earth* 5, 163–179 (doi:10.5194/se-5-163-2014)
- 971
- 972 Williams, I.S., 2001. Response of detrital zircon and monazite, and their U–Pb isotopic systems, to regional  
973 metamorphism and host-rock partial melting, Cooma Complex, southeastern Australia. *Australian Journal*  
974 *of Earth Sciences* 48, 557-580.
- 975
- 976 Woodland, B. G., 1963. A petrographic study of thermally metamorphosed pelitic rocks in the Burke area,  
977 northeastern Vermont. *American Journal of Science* 261, 354-375.
- 978
- 979 Zen, E.A., 1986. Aluminum enrichment in silicate melts by fractional crystallization: some mineralogic and  
980 petrographic constraints. *Journal of Petrology* 27, 1095-1117.

981

982 Zen, E.A., 1988. Phase relations of peraluminous granitic rocks and their petrogenetic implications. Annual  
 983 Review of Earth and Planetary Sciences 16, 21-51.

984

985 **TABLE CAPTIONS**

986 Table 1. Data from previous studies on igneous units in NW New Guinea.

987

988 **FIGURE CAPTIONS**

989 Figure 1. Overview of the study area. A: Tectonic map of eastern Indonesia and New Guinea. The red frame  
 990 delineates the location of subfigure B. B: Simplified geological map of NW New Guinea specifying granitoid  
 991 intrusions in the area and respective sample locations and numbers. The red rectangle delineates the  
 992 location of the geological map of Figure 2.

993

994 Figure 2. Geological map of the NE Kemum Basement High specifying sample locations and numbers.  
 995 Sampling locations for the Wasiani Granite (alluvial samples BJ92, and BJ93), the Kwok Granite (in-situ  
 996 sample BJ67), and the Momi Gabbro are indicated. Bold numerals refer to sample numbers (shorthand for  
 997 BJXXX, where XXX is the sample number; 5B and 6D refer to samples LW13-5B and LW13-6D,  
 998 respectively); regular numerals refer to waypoint numbers (shorthand for BH15-YYY, where YYY is the  
 999 waypoint number; exceptions BH14-16, BH14-17 and BH14-24 are indicated). Geology modified from  
 1000 Pieters et al. (1990) and Robinson et al. (1990c). Gb: Gabbro, Gt: Granite.

1001

1002 Figure 3. Granitoid exposures and field relationships in the E Kemum Basement High. A: Thin  
 1003 quartzofeldspathic sill offset by normal-separation faults (red lines) (waypoint BH15-083). B: Pegmatite  
 1004 dyke obliquely crosscutting metasedimentary basement rocks (waypoint BH15-142). After intrusion, the  
 1005 dyke was first folded and later boudinaged. Note the narrow dark aureole of contact metamorphism  
 1006 adjacent to the intrusion. C: Mingling indicated by cusped-lobate boundaries (left) and cross-cutting  
 1007 relationships indicated by straight and parallel boundaries (right) between the Momi Diorite (blue line)  
 1008 and the Anggi Granite. The Anggi Granite contains abundant country-rock xenoliths (dashed white line).  
 1009 The outcrop is cut by later normal-separation faults (red lines) (waypoint BH15-171). D: Pinch-and-swell  
 1010 structures of metapsammitic to metapelitic country rock xenoliths (dashed white line) in the Anggi

1011 Granite offset by normal-separation faults (red lines). The blue line denotes the contact of the Anggi  
1012 Granite with a metacalcareous country rock (waypoint BH15-174).

1013

1014 Figure 4. Representative photomicrographs of selected Devonian–Carboniferous (A–F, blue) and  
1015 Permian–Triassic granitoids (G–L, green). B: The Ngemona Granite with tourmaline (trm) overgrown by  
1016 garnet (gt) and muscovite (mu) surrounded by quartz (qtz), PPL (sample BJ53). B: The Wasiani Granite  
1017 with biotite next to sericitised plagioclase (plag), microcline (mic), and quartz; note the large zircon  
1018 crystal (blue arrow), PPL (sample BJ92). C: Monzonite associated with the Wasiani Granite showing a  
1019 glomerocryst of K-feldspar (kfs), amphibole, and chlorite, surrounded by K-feldspar in a fine-grained  
1020 groundmass of amphibole (blue arrow), chlorite, and K-feldspar, PPL (sample BJ93). D: Pegmatite  
1021 associated with the Wasiani Granite showing a broken crystal of kyanite (ky), partially replaced by white  
1022 mica at the top left corner (blue arrow) surrounded by quartz, muscovite, and subordinate plagioclase,  
1023 PPL (sample BJ104A). E: Kwok Granite with garnet, sericitised feldspar, quartz and biotite altering to  
1024 sillimanite (fibrolite, sill), PPL (sample BJ67). F: Melaiurna Rhyolite with phenocrysts of embayed quartz,  
1025 altered K-feldspar, saussuritized plagioclase, and bent muscovite (blue arrows) in a microcrystalline  
1026 groundmass, PPL (sample BJ22). G: A vein of secondary muscovite (green arrow) in a brittlely deformed  
1027 pegmatite containing plagioclase, microcline, and quartz associated with the Wariki Granodiorite, XPL  
1028 (sample BJ01). Note the kinking and deformation twinning in plagioclase. H: Granite of the Anggi Intrusive  
1029 Complex (AIC) showing garnet overgrown by biotite (green arrow) next to quartz and feldspar, PPL  
1030 (sample BJ138). I: Diorite of the Anggi Intrusive Complex with partially sericitised plagioclase  
1031 surrounding glomerocrysts of chlorite (alteration product of biotite), associated with abundant titanite  
1032 (green arrow), PPL (sample BJ134). J: High-alumina diorite associated with the Anggi Intrusive Complex  
1033 showing metastable hornblende (hbl) reacting to chlorite (bottom left) and garnet associated with biotite  
1034 (green arrow); plagioclase is the dominating felsic mineral, PPL (sample LW13-6D). K: Momi Gabbro with  
1035 abundant augitic pyroxene (cpx) overgrown by rims of amphibole (uralite, green arrows), plagioclase  
1036 laths, and minor biotite and quartz, XPL (sample LW13-5B). L: Kwatisore Granite with hornblende and  
1037 biotite surrounded by predominantly plagioclase, K-feldspar, and quartz, PPL (sample 12JD339A). Unit  
1038 names are indicated; Gb: Gabbro, Gdt: Granodiorite, Gt: Granite.

1039

1040 Figure 5. Microstructures of the granitoids. A: Fresh rims of plagioclase around older, partly sericitised  
 1041 plagioclase cores (core-and-mantle structures, blue arrows) where in contact with microcline; bulging  
 1042 recrystallization between microcline grains (red arrow) and grain boundary migration recrystallization  
 1043 between quartz and microcline (pinning, green arrow); trm: tourmaline, XPL. B: Myrmekite (blue arrow)  
 1044 in plagioclase (plag) where the mineral replaced microcline (mic) and consertal texture between quartz  
 1045 (qtz) and microcline (red arrow), XPL. C: Preferential growth of fibrolite microlites on a biotite crystal  
 1046 (bt), gt: garnet, PPL. D: Preferential replacement of muscovite (mu) with symplectites along {001}  
 1047 cleavage planes where in contact with plagioclase, but not where in contact with quartz, XPL. E: Large  
 1048 quartz grain with chessboard subgrains replaced by smaller quartz grains showing grain boundary  
 1049 migration and minor subgrain rotation recrystallization, XPL. F: Flame perthite (blue arrows), circular  
 1050 quartz exsolution features, and subordinate bulbous myrmekites (red arrow) in microcline, XPL. Sample  
 1051 numbers are indicated; Gdt: Granodiorite, Gt: Granite.

1052

1053 Figure 6. Migmatites observed in situ in the E Kemum Basement High. A: Pockets of neosome in an  
 1054 incipient migmatite associated with the Kwok Granite. B: Photomicrograph of the melanosome of A,  
 1055 showing restitic cordierite (crd) overgrowing sillimanite (red arrow), surrounded by quartz (qtz), biotite  
 1056 (bt), and plagioclase (blue arrow). C: Schlieric migmatite associated with the Anggi Intrusive Complex. D:  
 1057 Photomicrograph of C showing the melanosome with biotite and metastable muscovite (mu) in contact  
 1058 with large neoblasts of plagioclase (plag) and quartz representing the neosome. Sample numbers and  
 1059 sampling localities are indicated.

1060

1061 Figure 7. Harker-type variation diagrams for major elements of the granitoids of NW New Guinea. Iron is  
 1062 given as total ferrous iron (FeO<sub>T</sub>). Sample BJ83 is not dated (black triangle). Data for the Netoni Intrusive  
 1063 Complex (IC) are from Webb and White (2016). Gb: Gabbro, Gt: Granite, Gdt: Granodiorite, IC: Intrusive  
 1064 Complex, Ry: Rhyolite.

1065

1066 Figure 8. Peraluminosity of granitoids from NW New Guinea. A: Aluminium Saturation Index (ASI) vs.  
 1067 A/NK plot (Shand, 1927). B: AFM triangle for granitoids (Miller, 1985); Ps: strongly peraluminous, Pw:  
 1068 weakly peraluminous, Mw: weakly metaluminous. als: aluminosilicate, mu: muscovite, crd: cordierite, gt:  
 1069 garnet, bt: biotite, hbl: hornblende.

1070

1071 Figure 9. Trace element spidergrams normalised to the primitive mantle of Palme and O'Neill (2014). The  
1072 area shaded in grey delineates the composition of higher-grade basement rocks of the Kemum Formation  
1073 (n = 10); the area surrounded by a dashed line represents the composition of the Netoni Intrusive  
1074 Complex (Webb and White, 2016).

1075

1076 Figure 10. Summary of LA-ICP-MS U–Pb zircon data and ages for samples of Devonian–Carboniferous age.  
1077 Vertical bars represent the uncertainty (propagated 2s) of individual measurements. Filled bars represent  
1078 measurements used to calculate mean ages; empty bars represent rejected measurements. The coloured  
1079 line and ranges represent the weighted mean and both internal and propagated uncertainty (95% = 1.96  
1080 SDOM, standard deviation of the mean) of each sample.

1081

1082 Figure 11. Summary of LA-ICP-MS U–Pb zircon data and ages for samples of Permian–Triassic age (green).  
1083 Symbology as in Figure 10.

1084

1085 Figure 12. Representative CL images of zircon textures observed (A–D) and of selected examples of  
1086 rounded and concordant inherited cores (E–H). Many samples contain zircons with magmatic growth  
1087 zones (A, C, E, F, G, and H), while the zircons of some samples (especially the Ngemona, Kwok, and Wasiani  
1088 granites) are not zoned and often CL-bright (B); BJ93 is additionally characterised by angular and  
1089 xenomorph crystal shapes (B). Growth-zoned zircons from the Wariki Granodiorite were fractured and  
1090 subsequently 'cemented' with later (metamorphic?) zircon overgrowths (C). Care was taken to ablate only  
1091 the magmatic fragments of the zircons. Some evolved or pegmatitic samples (BJ08, BJ09, and BJ80) are  
1092 characterised by uniformly CL-dark zircons (D).  $^{207}\text{Pb}/^{206}\text{Pb}$  ages are reported for cores >1000 Ma (F–H);  
1093 note the large error of a core of sample LW13-5B (G). Ages in square brackets were not used to calculate  
1094 weighted mean ages.

1095

1096 Figure 13. Pre-Cenozoic granitoids in eastern Indonesia and Papua New Guinea. A: Global plate tectonic  
1097 reconstruction of the Late Triassic (modified from Metcalfe (2013)). The red circle marks the approximate  
1098 location of NW New Guinea at the time. B: Current map of dated pre-Cenozoic granitoids. C: Graphical  
1099 representation of the ages of the units in B, specifying the isotopic system used (K–Ar or U–Pb). Bold

1100 numbers correspond to the locations shown in B. Many of the cited publications are difficult to access, but  
1101 the data has been summarised by Davies (1990). Geological time scale after Gradstein et al. (2012).

1102

1103 **CAPTIONS TO THE SUPPLEMENTARY DATA FILES**

1104 Supplementary Data File 1. Granitoids of NW New Guinea: A literature review.

1105

1106 Supplementary Data File 2. Waypoints and samples used in this study.

1107

1108 Supplementary Data File 3. Qualitative modal composition of granitoid samples studied in thin section.

1109

1110 Supplementary Data File 4. Scanning electron microscope cathodoluminescence images of individual  
1111 samples analysed with LA-ICP-MS, indicating laser spots and integration numbers.

1112

1113 Supplementary Data File 5. U–Pb zircon LA-ICP-MS measurement parameters.

1114

1115 Supplementary Data File 6. Methodology and data treatment for U–Pb zircon dating.

1116

1117 Supplementary Data File 7. Petrography of the Devonian–Carboniferous and the Permian–Triassic  
1118 granitoids.

1119

1120 Supplementary Data File 8. XRF bulk rock analyses, CIPW norms, and ASI and A/CNK values used in this  
1121 study.

1122

1123 Supplementary Data File 9. Compilation of LA-ICP-MS data.

1124

1125 Supplementary Data File 10. Tera-Wasserburg diagrams for the samples presented in this study.

1126

1127 Supplementary Data File 11. Summary of calculated weighted mean age populations for the U–Pb data,  
1128 including uncertainties, MSWD, and number of analyses.

1129

- 1130 Supplementary Data File 12. Change of crystallisation age with increasing discordance for samples BJ08,  
1131 BJ09, and BJ80.

**Figure 1**

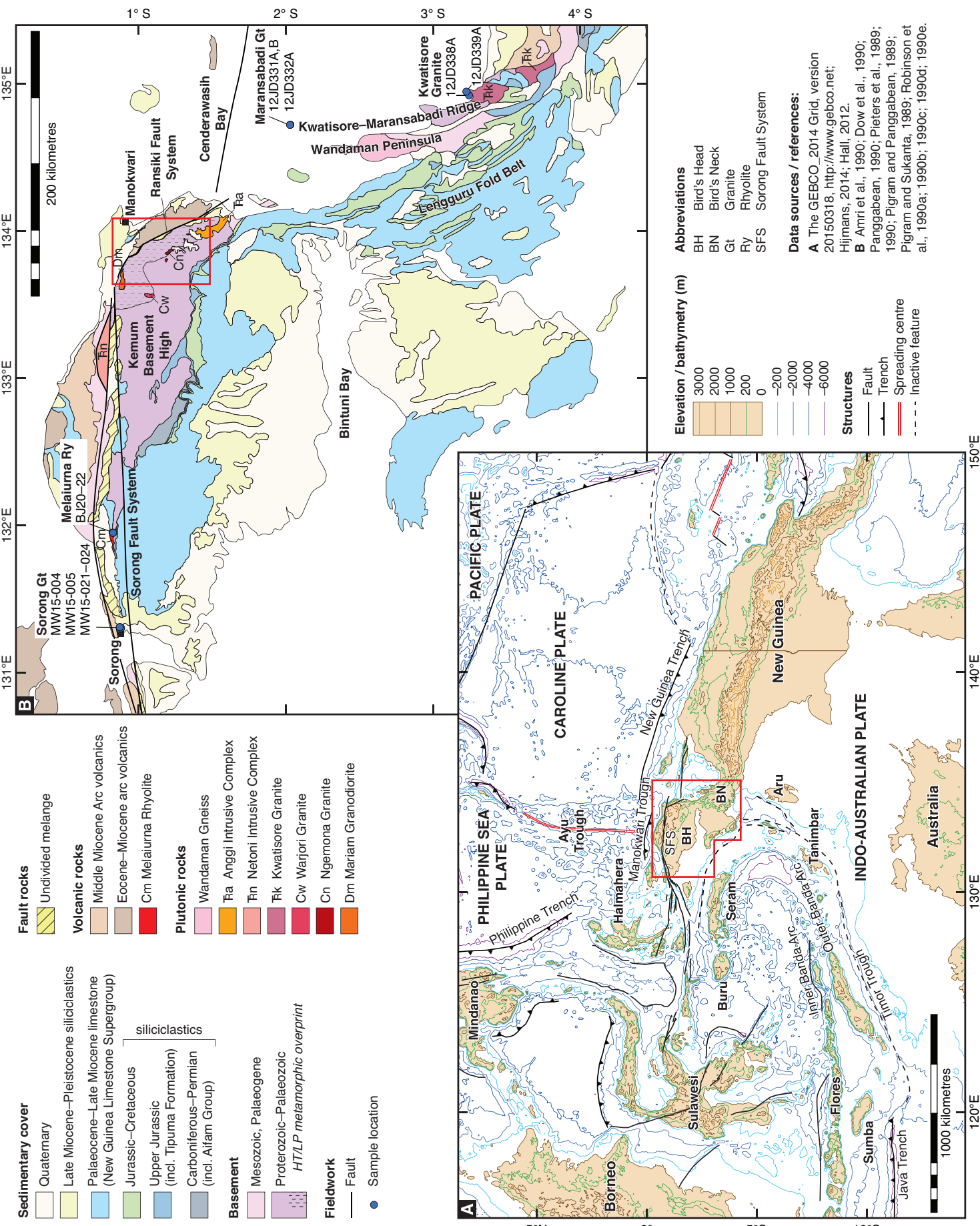


**Figure 2**

**Samples and Waypoints**

- Waypoint
- Sample, undated
- Sample, Permian–Triassic
- Sample, Carboniferous
- Sample, Devonian–Carboniferous
- Float sample, scree sample
- Tracks

- Fault (observed, approximate, covered)
- Q Quaternary

**RANSIKI FAULT SYSTEM**

- Tmle Lembai Diorite
- RFx Undivided melange

**ARFAK BLOCK**

- Qpm Manokwari Formation
- TQb Befoor Formation
- Tmma Maruni Limestone
- Tema Arfak Volcanics

**KEMUM BLOCK**

**Sedimentary cover**

- Qpme Menyambo Formation
- TQb Befoor Formation
- TQw Wai Formation
- New Guinea Limestone
- Tmka Kais Limestone
- Toms Sirga Formation
- Tef Faumai Limestone
- Kj Jass Formation
- RJt Tipuma Formation

**Intrusive rocks**

- Ra Anggi Granite
- Rw Wariki Granodiorite
- Cn Ngemona Granite
- Dm Mariam Granodiorite

**Basement**

- SDk Kemum Formation
- Biotite zone
- Andalusite zone

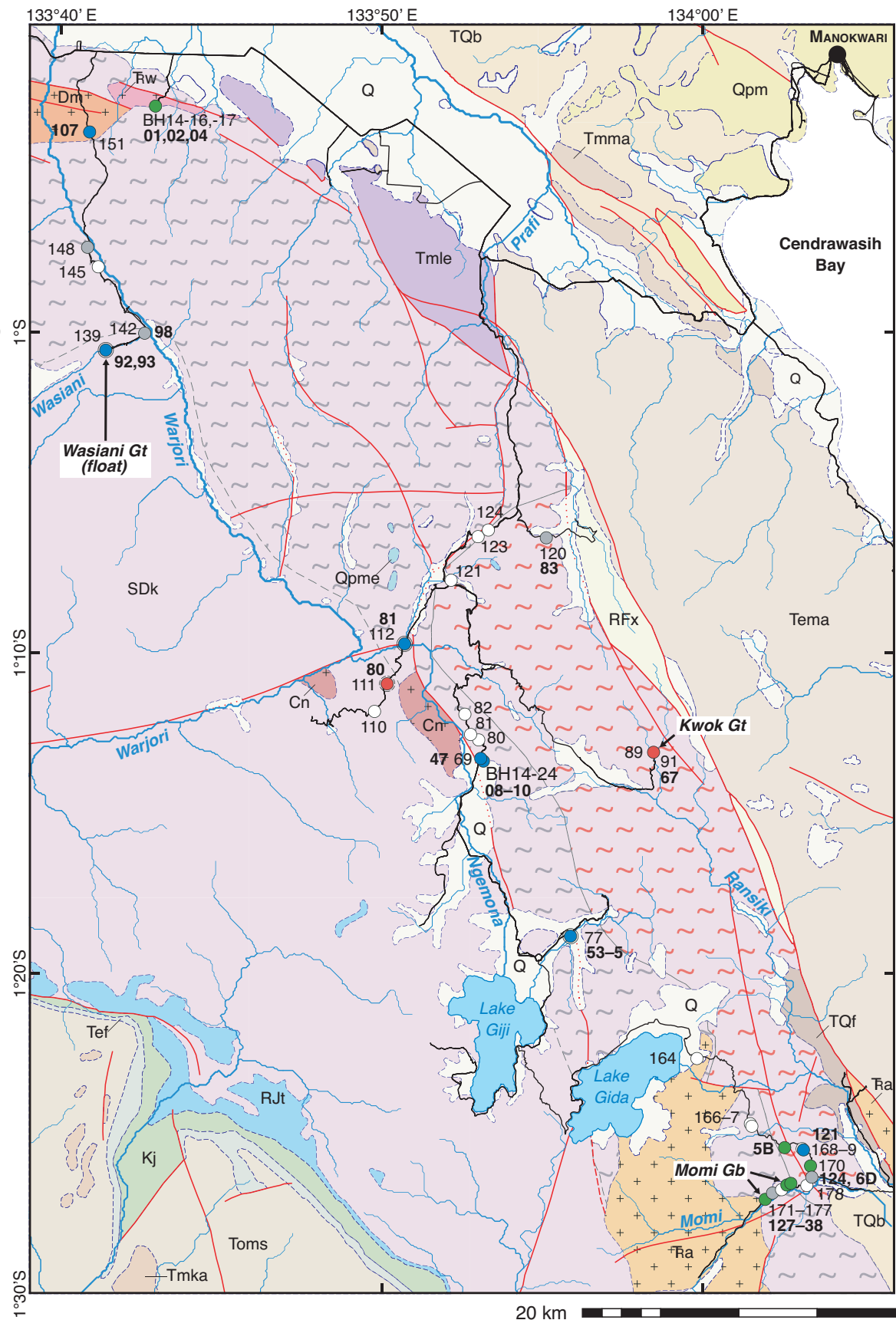


Figure 3  
[Click here to download high resolution image](#)

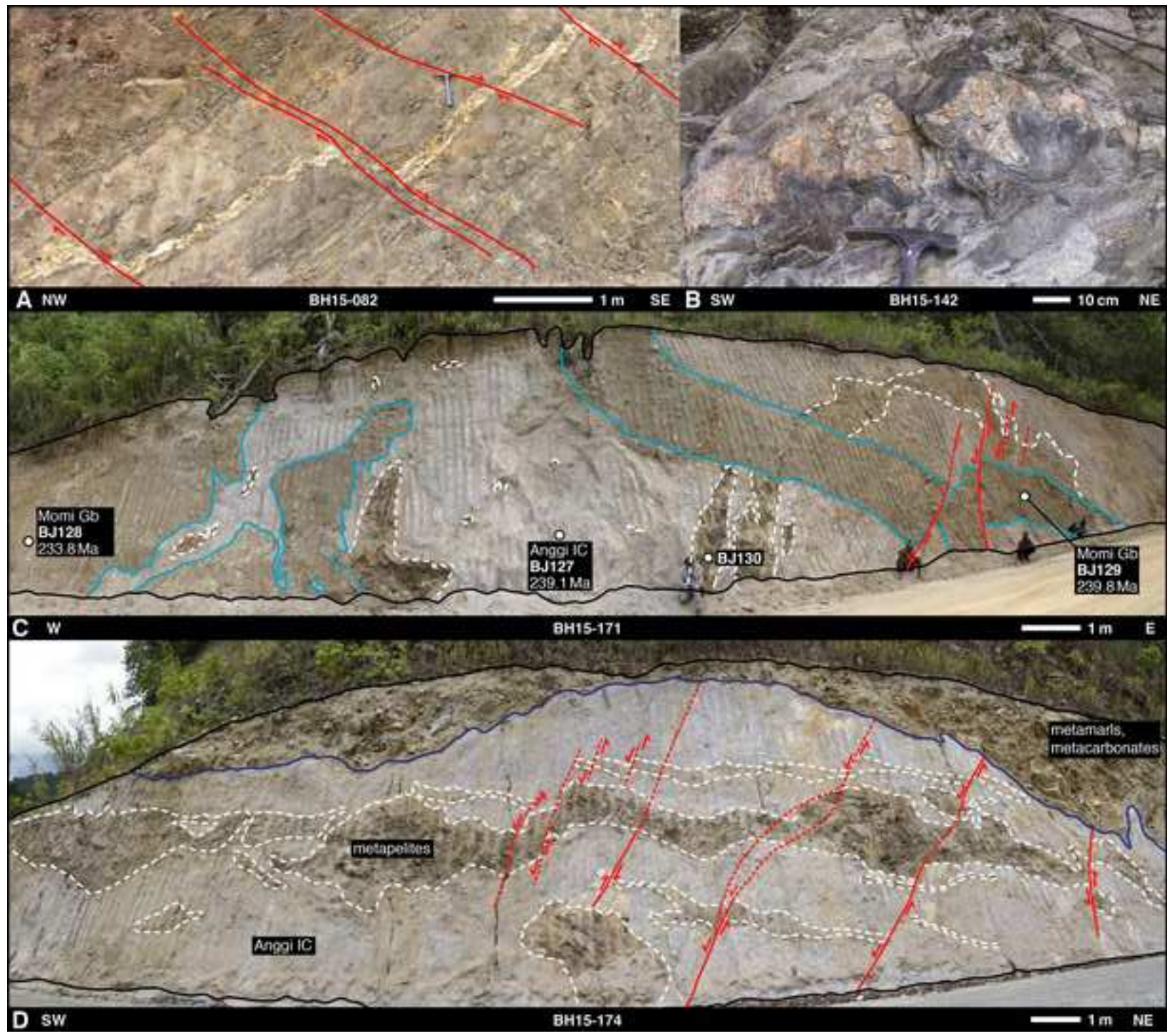


Figure 4  
[Click here to download high resolution image](#)

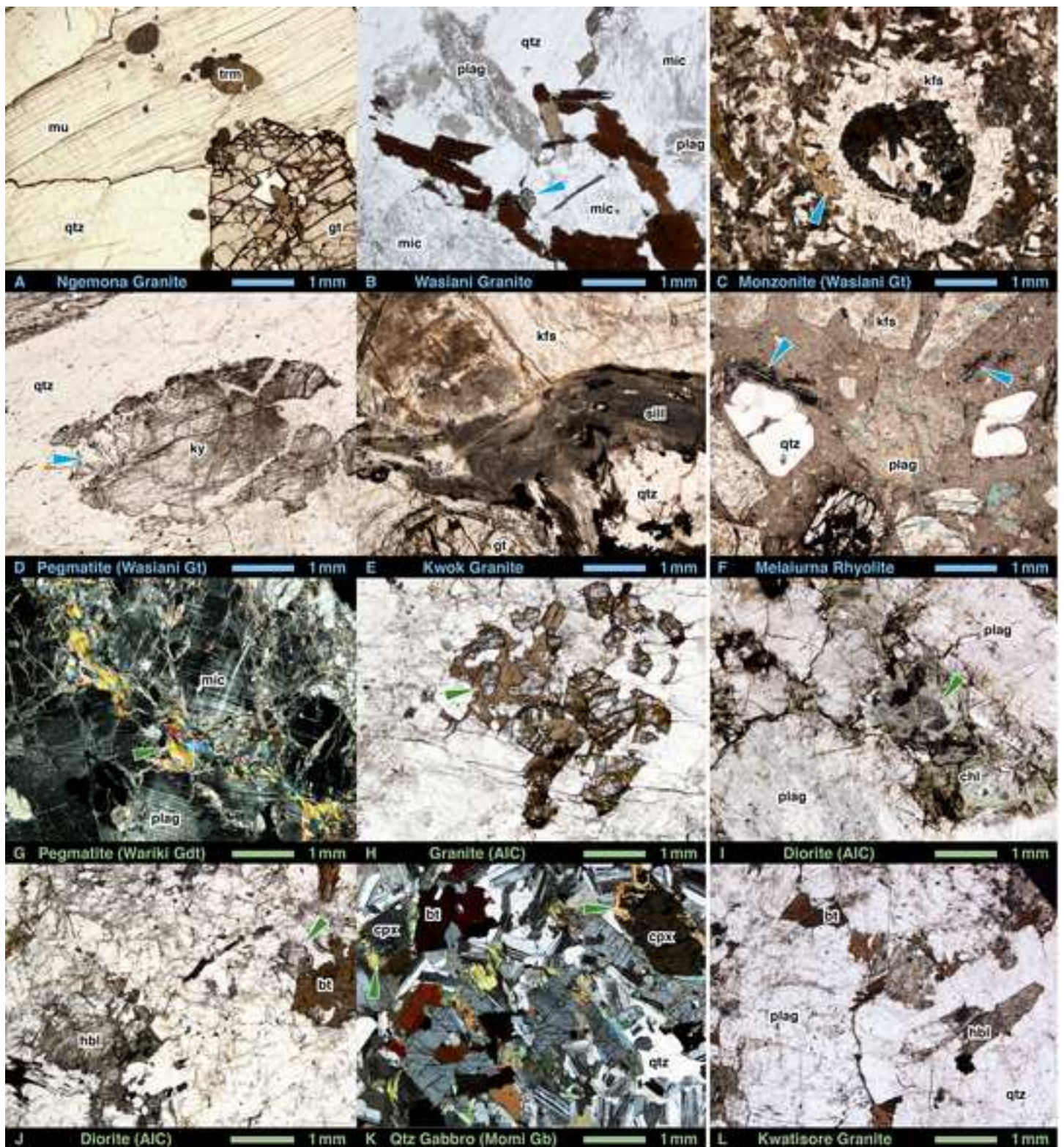


Figure 5  
[Click here to download high resolution image](#)

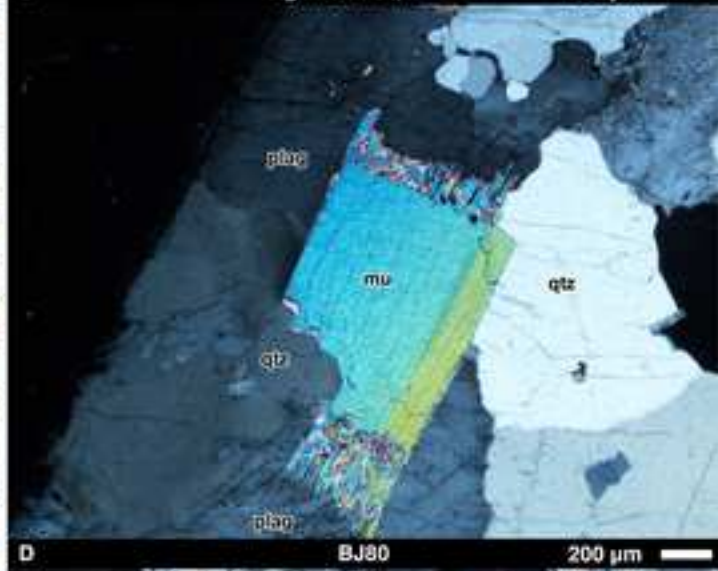


Figure 6  
[Click here to download high resolution image](#)

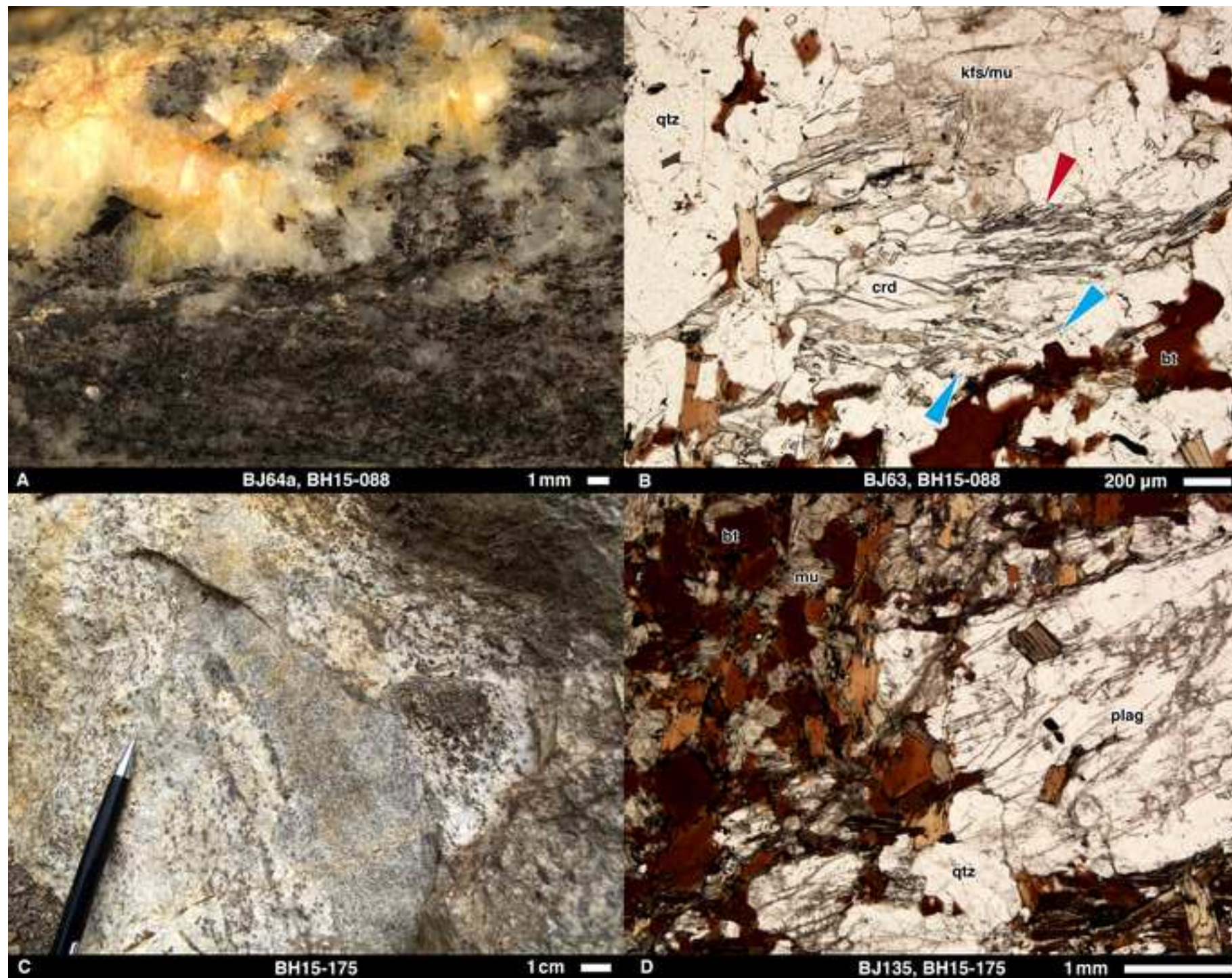
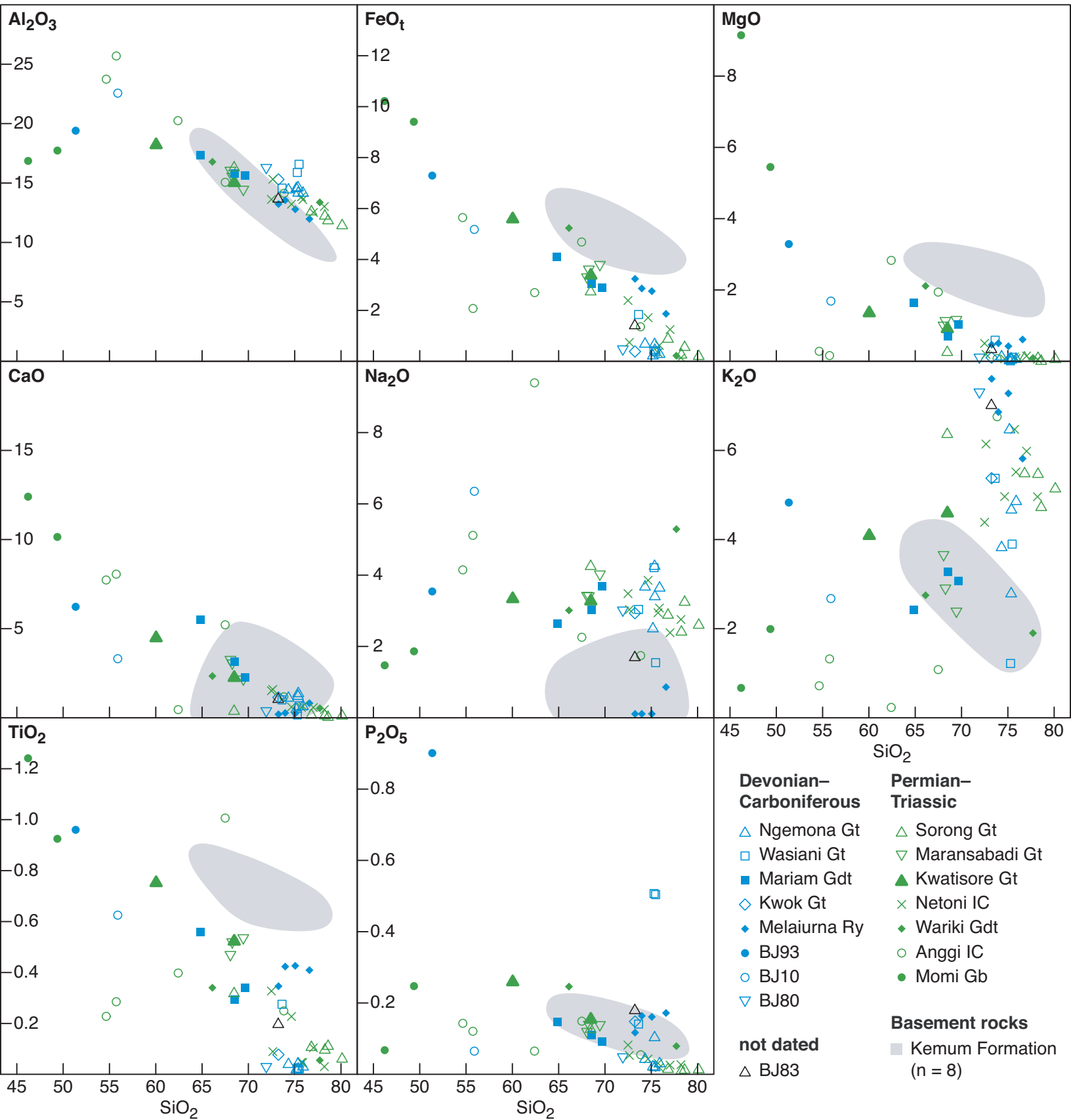
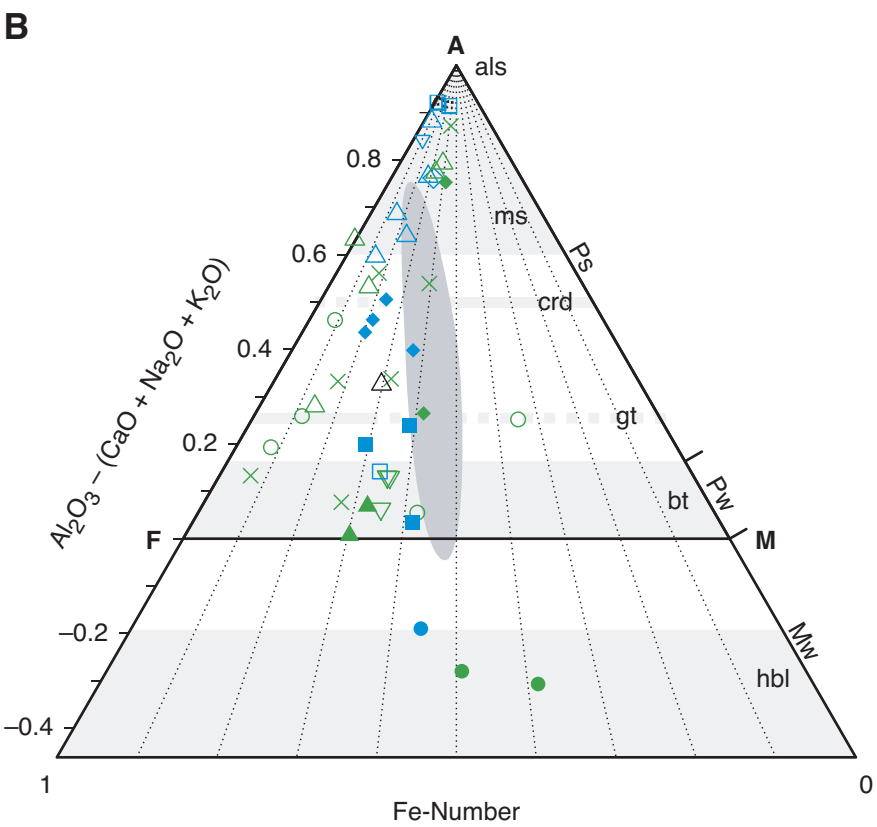
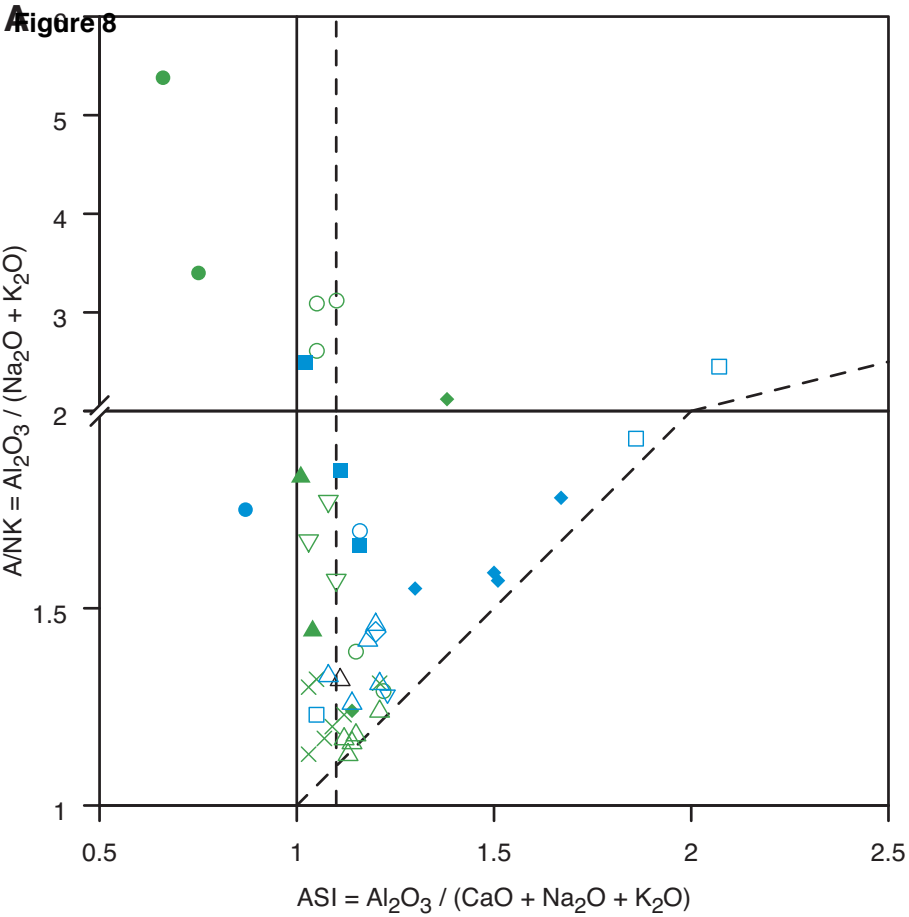


Figure 7





**Devonian–Carboniferous**

- △ Ngemona Gt
- Wasiani Gt
- Mariam Gdt
- ◇ Kwok Gt
- ◆ Melaiurna Ry
- BJ93
- BJ10
- ▽ BJ80

**Permian–Triassic**

- △ Sorong Gt
- ▽ Maransabadi Gt
- ▲ Kwatisore Gt
- × Netoni IC
- ◆ Wariki Gdt
- Anggi IC
- Momi Gb

**not dated**

- △ BJ83

**Basement rocks**

- Kemum Formation (n = 8)

Figure 9

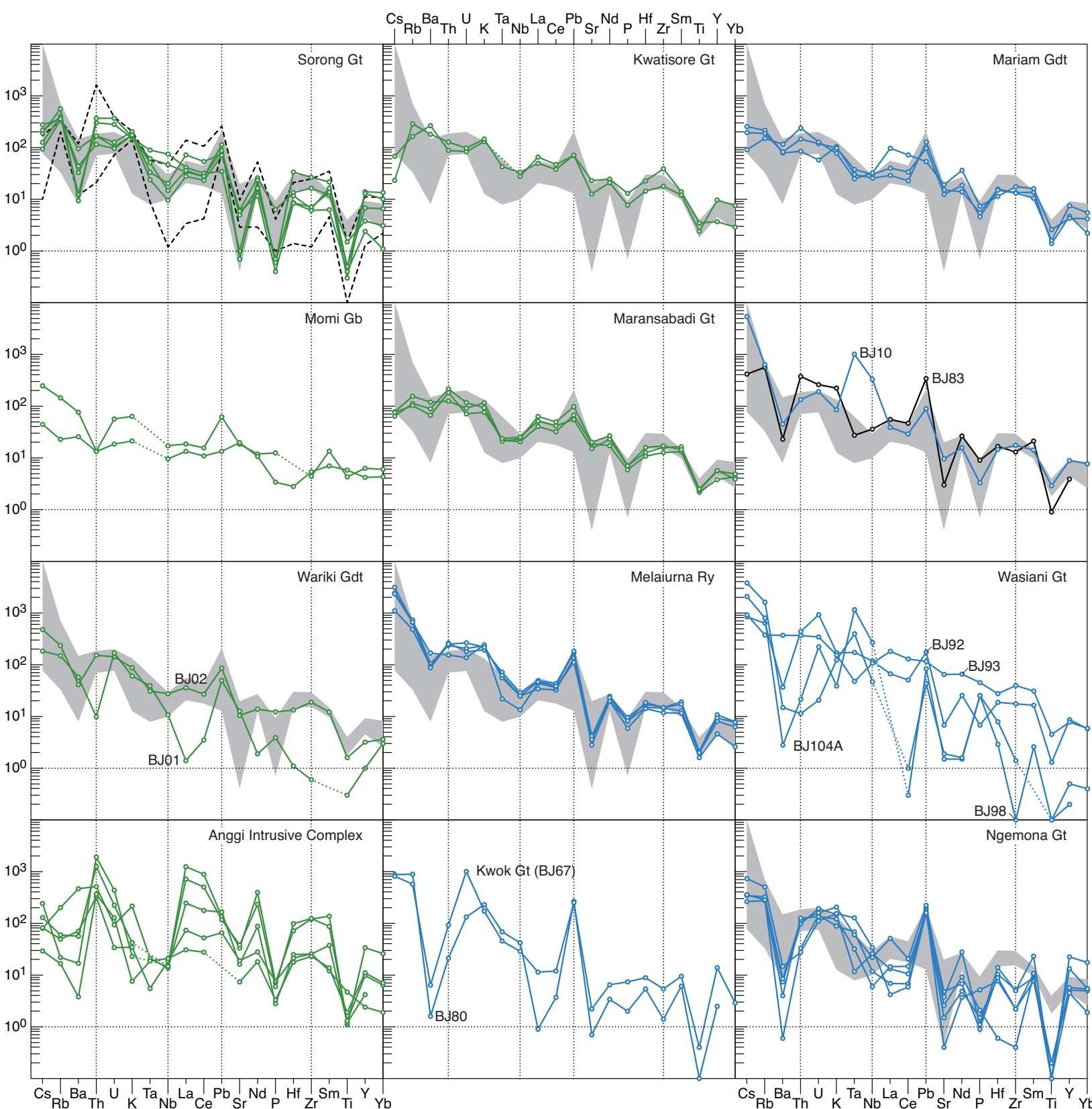


**Figure 10**

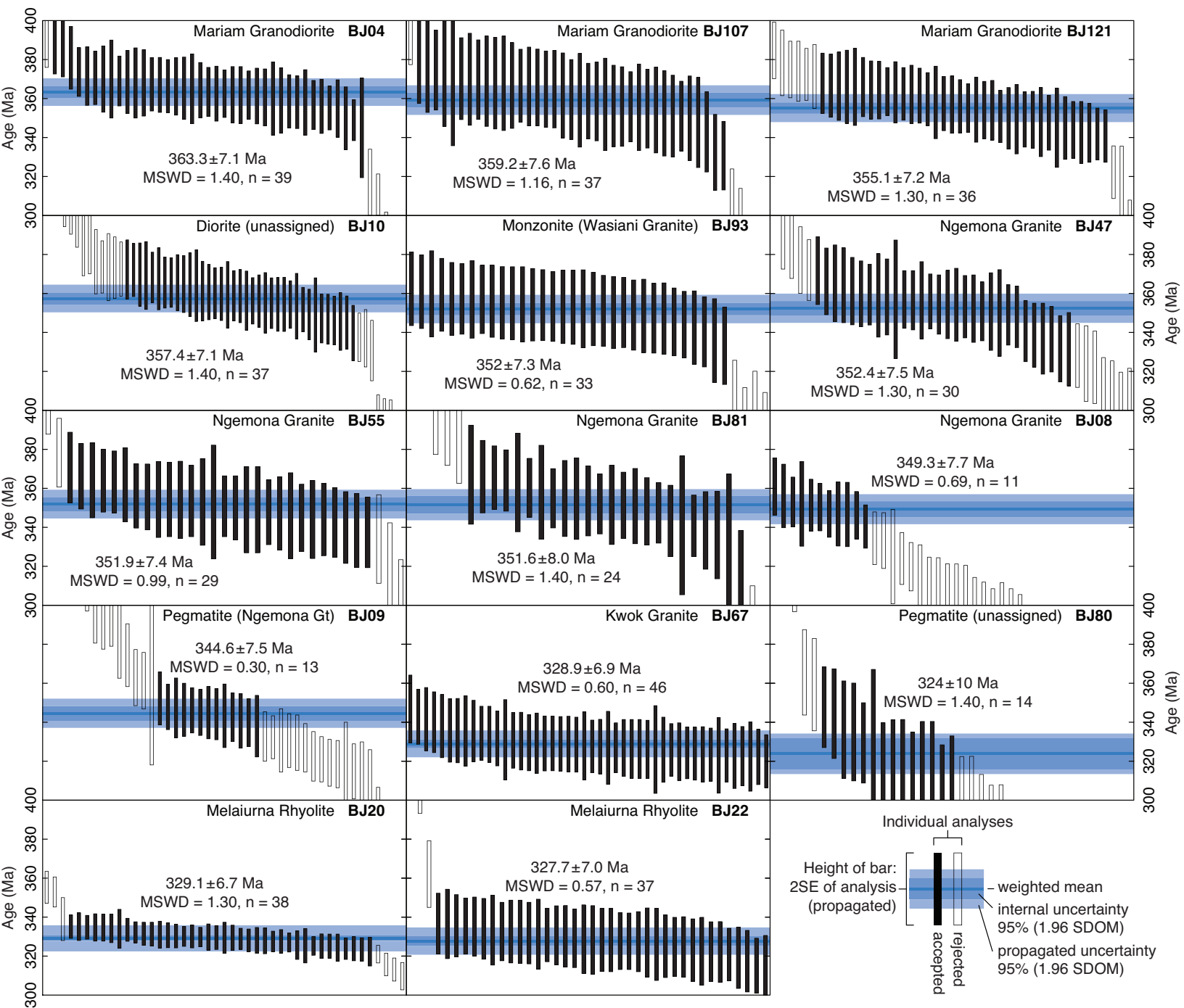


**Figure 11**

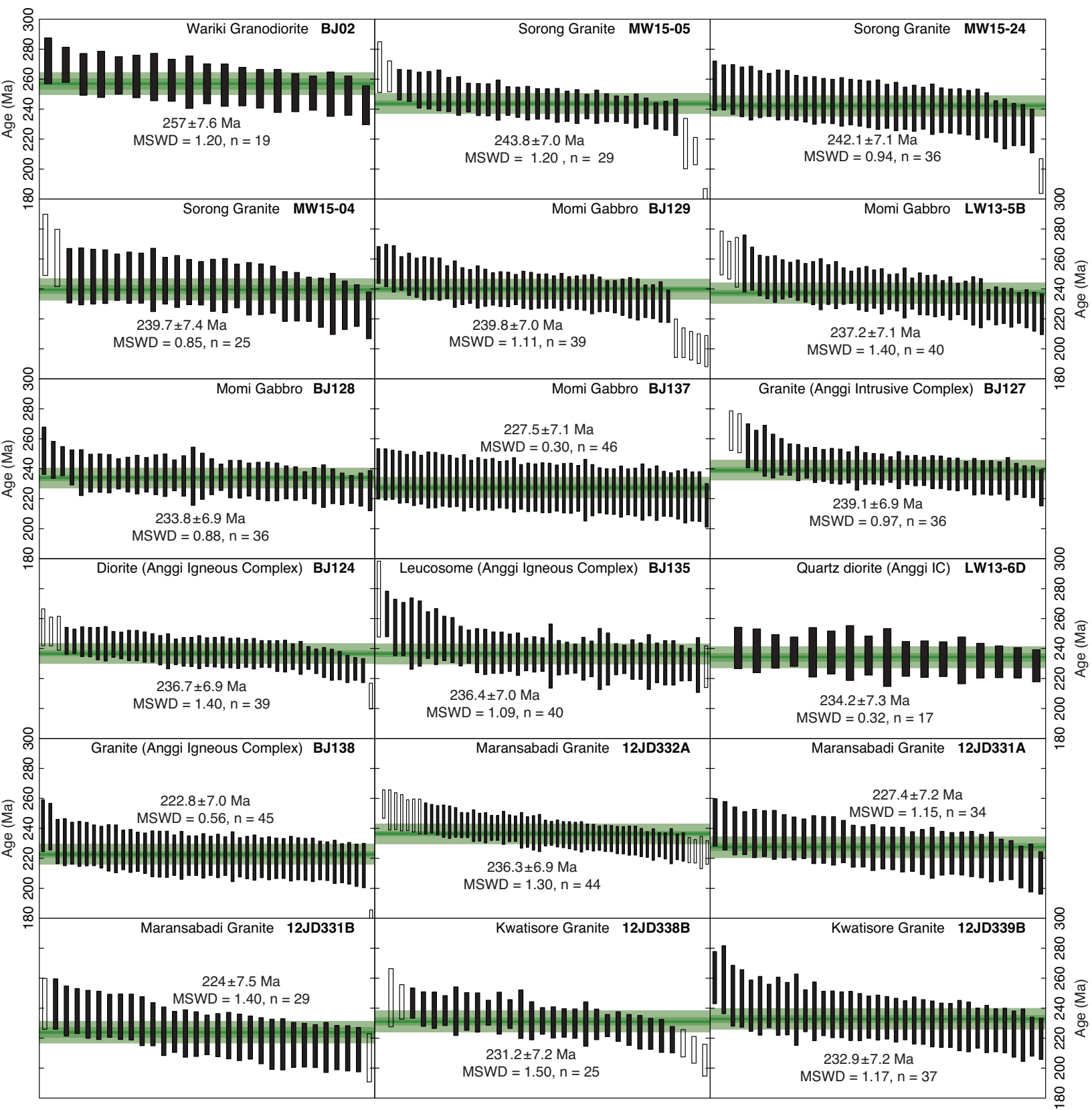
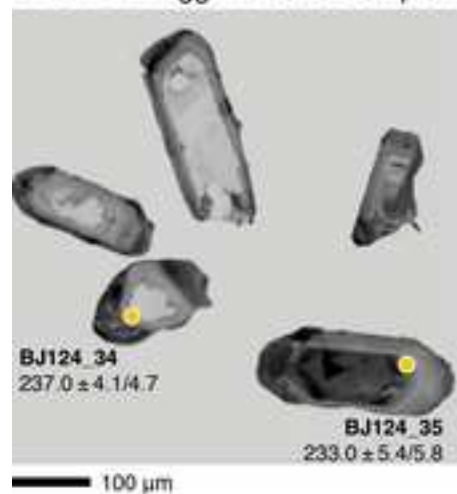


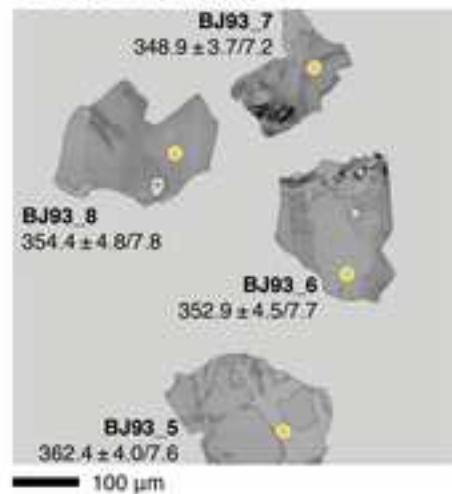
Figure 12  
[Click here to download high resolution image](#)

### General features

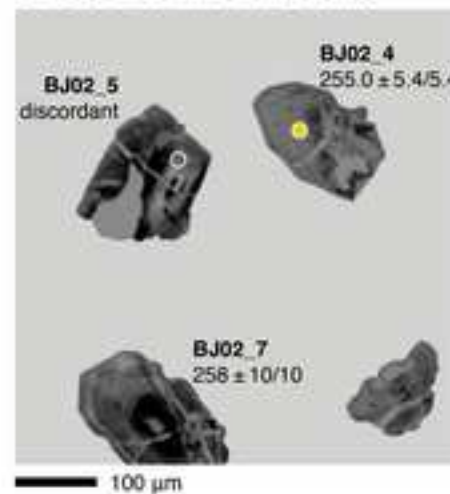
**A** BJ124 Anggi Intrusive Complex



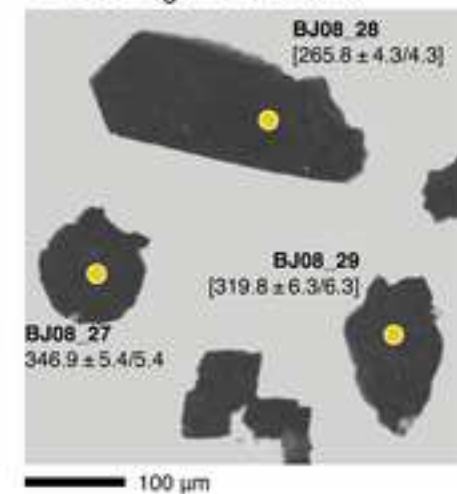
**B** BJ93 Monzonite



**C** BJ02 Wariki Granodiorite

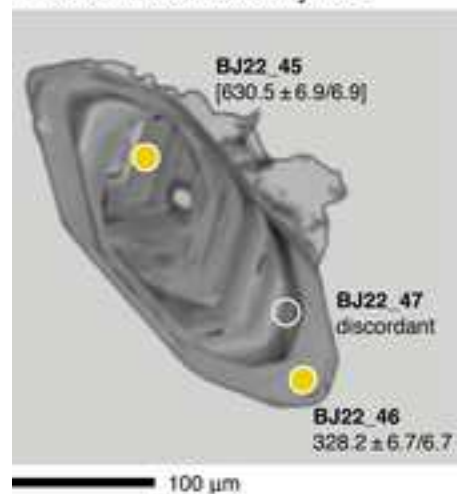


**D** BJ08 Ngemona Granite

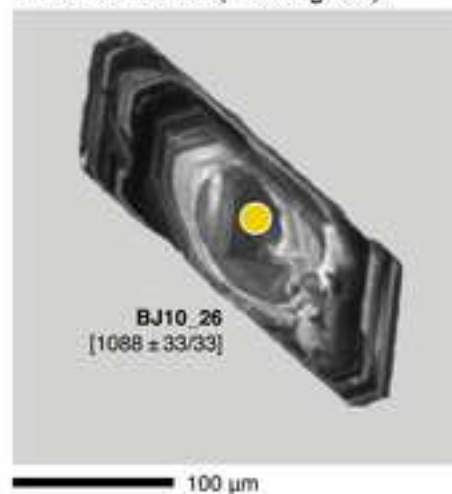


### Inherited cores

**E** BJ22 Melaiurna Rhyolite



**F** BJ10 Diorite (unassigned)



**G** LW13-5B Momi Gabbro

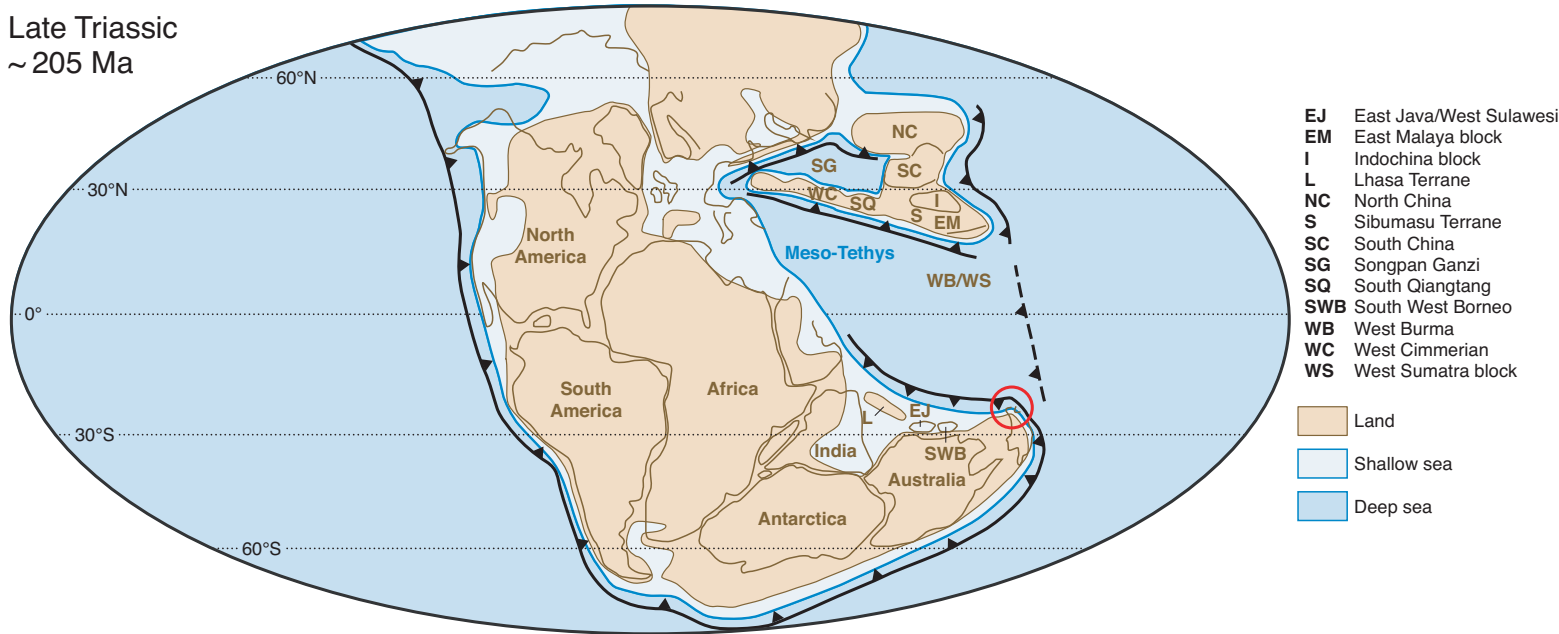


**H** BJ127 Anggi Intrusive Complex

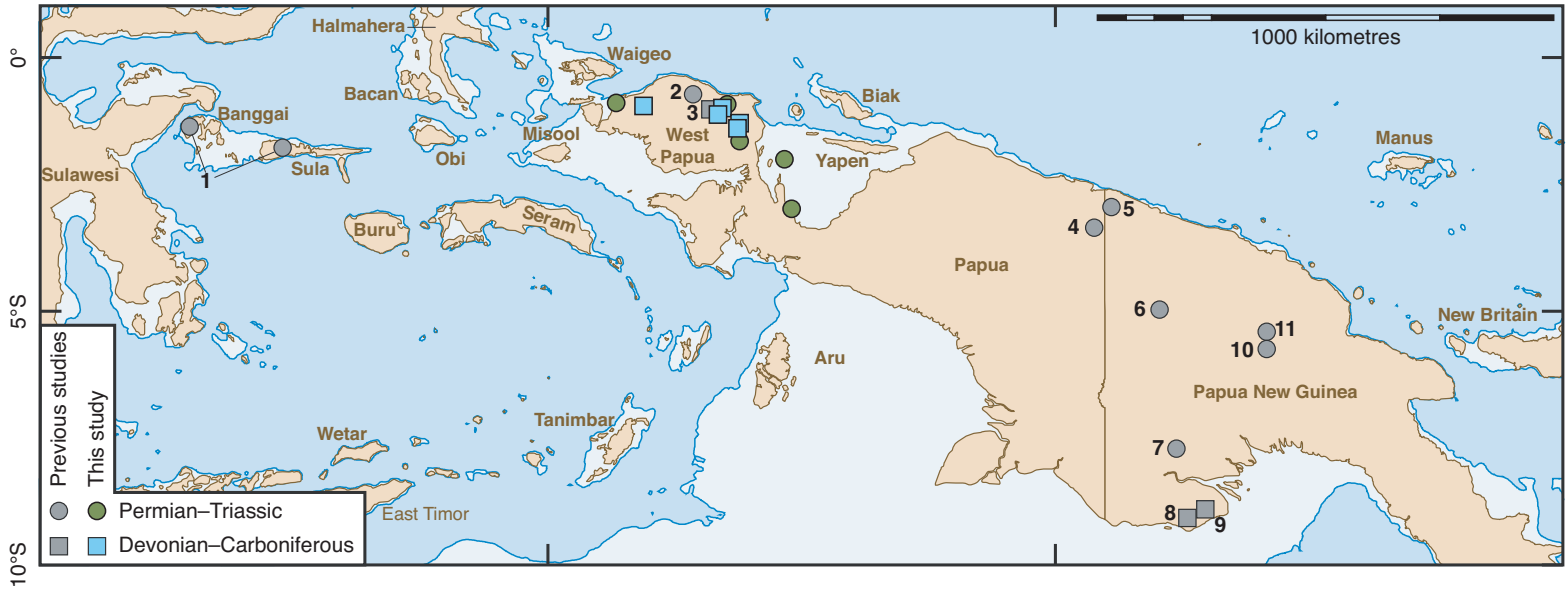


**Figure 13**

**A** Late Triassic  
~205 Ma



**B** 120°E 130°E 140°E 150°E



**C** 200 250 300 350 370 Ma

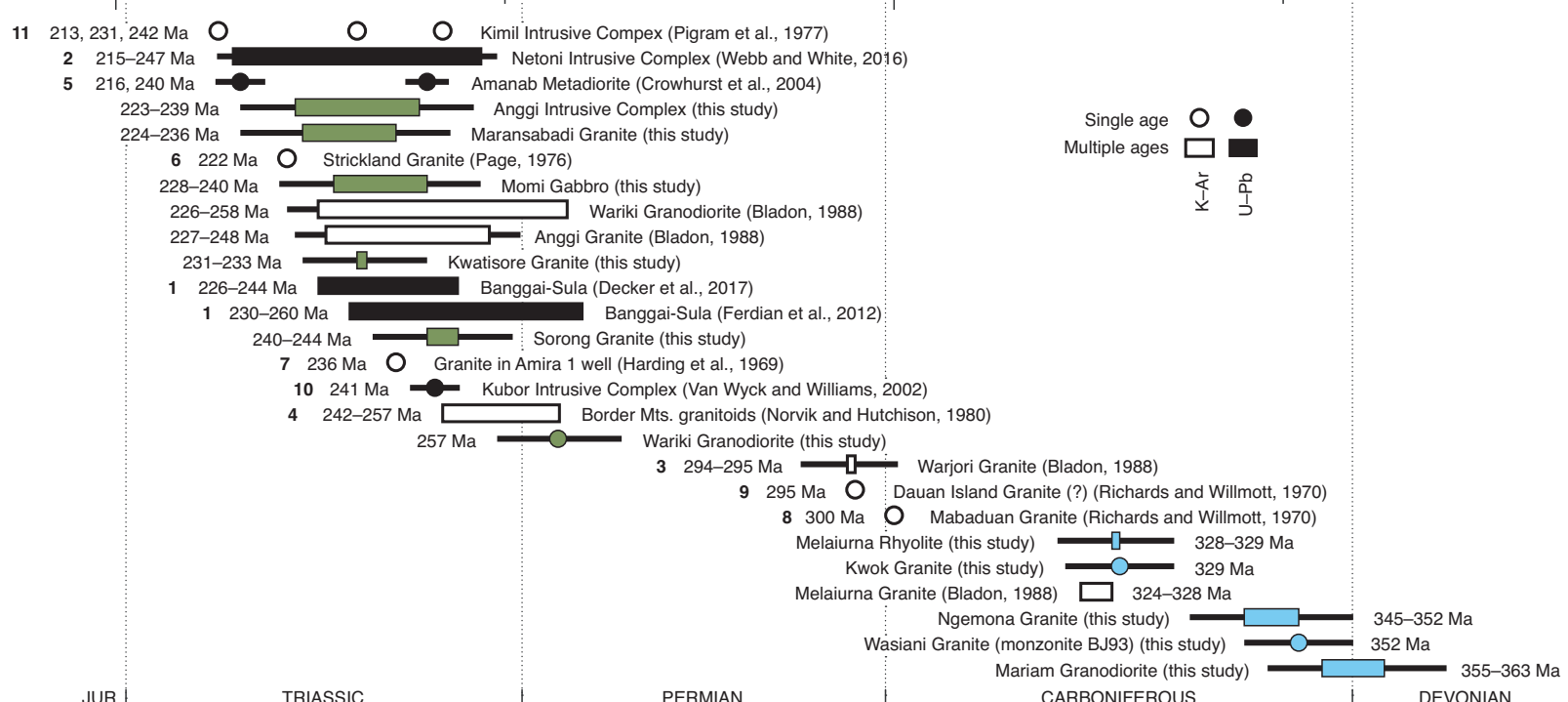


**Table 1**[Click here to download Table: Table1.docx](#)**Table 1** Data from previous studies on igneous units in NW New Guinea.

Unit	Description	Relations	Age (Ma)	N	System	Reference
Maransabadi Gt	Biotite granite or granodiorite, diorite, gabbro, rare tourmaline pegmatite	Emplaced in undifferentiated metasediments	278, 231	2 <sup>a</sup>	K-Ar	Bladon (1988), Pieters et al. (1983), Robinson et al. (1990d)
Kwatisore Gt	Grey biotite granite, pink two-feldspar granite	Intrudes and in faulted contact with undifferentiated metasediments; overlain by Miocene limestone and quartz sandstone	197±3	1 <sup>a</sup>	K-Ar	Bladon (1988), Pieters et al. (1983), Robinson et al. (1990e)
Sorong Gt	Red, equigranular granite, minor aplite, quartz veins; commonly sheared	In faulted contact with other units in the Sorong Fault System	224±11	1 <sup>b</sup>	K-Ar	Amri et al. (1990)
Netoni Intrusive Complex	Granite, granodiorite, quartz monzonite, and syenite with minor diorite, quartz diorite, and pegmatite; xenoliths of gabbro, diorite, amphibolite, and hornblende schist	Fault-bounded fragment (facoid) in the Sorong Fault System	256–206	5	U-Pb	Bladon (1988), Pieters et al., (1989), Webb and White (2016)
Wariki Gdt	Course-grained granodiorite with quartz, plagioclase, K-feldspar, biotite, and minor muscovite, accessory tourmaline, apatite, zircon, garnet, and allanite; subordinate monzogranite and tonalite; fine-grained, biotite-rich schlieren and xenoliths are common; locally cut by pegmatite and aplite dykes; variably deformed (cohesive cataclasites to ultramylonites)	Plutons in mainly faulted contact with Kemum Fm	258–222	6 <sup>c</sup>	K-Ar	Bladon (1988), Robinson et al. (1990c)
Anggi Gt <sup>d</sup>	Biotite and biotite-muscovite granite, subordinate quartz diorite; medium-grained; xenoliths and roof pendants of country rock as well as late-stage aplite and pegmatite dykes common; biotite-rich (mesocratic) xenoliths common along margins	Intrudes and in faulted contact with Kemum Fm; phacoids in Ransiki Fault System	248–225	3 <sup>a</sup>	K-Ar	Bladon (1988), Pieters et al. (1990)
Warjori Gt	Biotite granite; medium-grained	Intrudes Kemum Fm	295–294	2 <sup>a</sup>	K-Ar	Bladon (1988), Pieters et al. (1990)
Melaiurna Gt <sup>d</sup>	Pink porphyritic granites cut by dacite dykes; phenocrysts of quartz, plagioclase, K-feldspar, and biotite in a groundmass of quartz and feldspar.	Intrudes Kemum Fm, but is not metamorphosed; unconformably overlain by Aifam Gp	328–324	2 <sup>a</sup>	K-Ar	Amri et al. (1990), Bladon (1988), Visser and Hermes (1962)

Abbreviations: Gdt: granodiorite, Gt: granite, N: number of samples dated

<sup>a</sup> Description or age obtained from alluvial river detritus samples, no in-situ sample available<sup>b</sup> No information available regarding sample type or location<sup>c</sup> Four of the five samples of the Wariki Gdt are alluvial river detritus samples<sup>d</sup> Previous name; we renamed the units 'Anggi Intrusive Complex' and 'Melaiurna Rhyolite'

**Supplementary Data File 1**

[Click here to download Background dataset for online publication only: SuppDataFile1.pdf](#)

**Supplementary Data File 2**

[Click here to download Background dataset for online publication only: SuppDataFile2.pdf](#)

**Supplementary Data File 3**

[Click here to download Background dataset for online publication only: SuppDataFile3.pdf](#)

**Supplementary Data File 4**

[Click here to download Background dataset for online publication only: SuppDataFile4.pdf](#)

**Supplementary Data File 5**

[Click here to download Background dataset for online publication only: SuppDataFile5.pdf](#)

**Supplementary Data File 6**

[Click here to download Background dataset for online publication only: SuppDataFile6.pdf](#)

**Supplementary Data File 7**

[Click here to download Background dataset for online publication only: SuppDataFile7.pdf](#)

**Supplementary Data File 8**

[Click here to download Background dataset for online publication only: SuppDataFile8.xlsx](#)

**Supplementary Data File 9**

[Click here to download Background dataset for online publication only: SuppDataFile9.xlsx](#)

**Supplementary Data File 10**

[Click here to download Background dataset for online publication only: SuppDataFile10.pdf](#)

**Supplementary Data File 11**

[Click here to download Background dataset for online publication only: SuppDataFile11.pdf](#)

**Supplementary Data File 12**

[Click here to download Background dataset for online publication only: SuppDataFile12.pdf](#)